CHALMERS
UNIVERSITY OF TECHNOLOGY

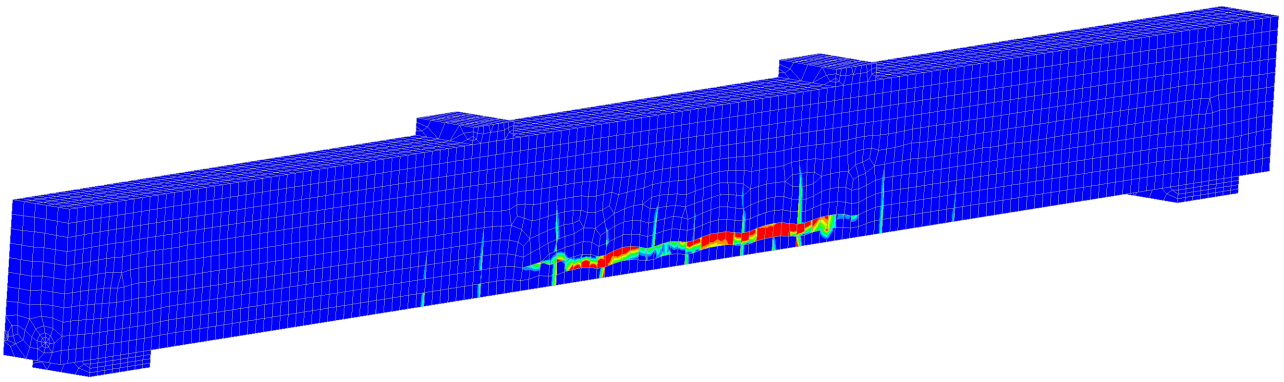

FE Analysis on the Interconnection between Bending and Corrosion-Induced Cracks

Jonathan Thorsson

Department of Architecture and Civil Engineering
CHALMERS UNIVERSITY OF TECHNOLOGY
Gothenburg, Sweden 2023

Master's thesis ACEX30

FE Analysis on the Interconnection between Bending and Corrosion-Induced Cracks

Jonathan Thorsson

CHALMERS
UNIVERSITY OF TECHNOLOGY

Department of Architecture and Civil Engineering
Division of Structural Engineering
Research group: Concrete Structures
Chalmers University of Technology
Gothenburg, Sweden 2023

FE Analysis on the Interconnection between Bending and Corrosion-Induced Cracks

Jonathan Thorsson

Supervisors: Professor Karin Lundgren, postdoctoral researcher Langzi Chang, Department of Architecture and Civil Engineering
Examiner: Professor Karin Lundgren, Department of Architecture and Civil Engineering

Department of Architecture and Civil Engineering
Division of Structural Engineering
Research group: Concrete Structures
Chalmers University of Technology
SE-412 96 Gothenburg
Telephone +46 31 772 1000

Cover: An illustration of crack width output for a beam under four-point bending and corrosion.

Department of Architecture and Civil Engineering
Gothenburg, Sweden 2023

To mom and Dad

FE Analysis on the Interconnection between Bending and Corrosion-Induced Cracks
JONATHAN THORSSON
Department of Architecture and Civil Engineering
Division of Structural Engineering
Research group: Concrete Structures
Chalmers University of Technology

Abstract

Reinforced concrete structures degrade due to carbonation or chloride-induced corrosion. As these structures age, understanding corrosion-induced damage becomes more important. When reinforcement within concrete corrodes, it generates corrosion products that occupy more space than the original steel. Confined within the concrete, these products exert pressure, causing stress accumulation and subsequent cracking. Previous investigations on pitting corrosion and formation of longitudinal cracks in reinforced concrete beams have yielded inconsistent results, highlighting the uncertain relationship between pitting corrosion and corrosion-induced cracks. While some studies have used finite element analysis to assess concrete cracking caused by corrosion, few have explored the consequences of reinforced concrete beams undergoing imposed deformation during the corrosion process. This thesis presents non-linear finite element analyses of crack patterns and crack widths in a reinforced concrete beam experiencing chloride-induced corrosion and imposed deformation, including bending cracks. The results are compared with experimental data. The analysis considers different types and degrees of corrosion distribution, as well as varying the volume expansion of corrosion products. The finite element analyses successfully replicated the observed corrosion-induced crack pattern on the beam's lateral side. Corrosion induced cracks initiated both at the bending cracks, and between the bending cracks when both uniform and pitting corrosion was considered. When pitting corrosion was removed or kept constant, corrosion induced cracks was initiated primarily between the bending cracks. Pitting corrosion was identified as a factor that increased longitudinal crack widths at the pit location, with its influence diminishing further away. Moreover, the analysis supported the experimental results, that the most corroded section does not necessarily result in the largest crack widths. Additionally, it revealed the non-linear effects of volume expansion and change in crack widths. A small increase in volume expansion could lead to a significant increase in crack widths and crack widths could increase more at one location and less in others. The FE analysis did reproduce the linear crack growth observed in the experiment when the crack widths are small. Future work should focus on including more test data with varying levels of imposed deformation and examining corrosion rate, corrosion product dissipation, and the impact of stirrups on corrosion-induced cracking. Additionally, running less varied FE analyses in scenarios where the bending cracks and pit locations are more controlled can provide valuable insights into their effect on measured crack widths.

Keywords: Reinforced concrete structures, finite element analysis, chloride-induced corrosion, crack pattern, crack width, corrosion distribution, volume expansion

Acknowledgements

I would like to express my sincerest gratitude to Professor Karin Lundgren, who served as my supervisor and examiner, as well as to my second supervisor, postdoctoral researcher Langzi Chang for their unwavering support and vast expertise have been invaluable throughout the entire process of completing this thesis. Professor Lundgren's commitment to imparting knowledge and her genuine care for her supervisees play a pivotal role in making these projects possible. Her guidance and encouragement have been instrumental in shaping my understanding and approach to the subject matter. I am truly grateful for her dedication. I would also like to acknowledge the significant contributions of Langzi Chang, whose expertise and assistance were crucial in creating and implementing the finite element model utilized in this thesis. His support and guidance have greatly enhanced the quality of my research. I extend my best wishes to Langzi and Karin for all their future endeavors.

Special thanks are due to Carlos Berrocal, Ignazi Fernandez, and Rasmus Rempling for their previous work conducting the experiment on which this thesis is based.

I would like to express my wholehearted appreciation to my girlfriend during this project for her unwavering support and understanding. Also extend my thanks to friends and family for their encouragement during all my years of study at Chalmers.

Jonathan Thorsson, Gothenburg, June 2023

Contents

List of Figures

List of Tables

1

Introduction

1.1 Background

Since the inception of reinforced concrete in the mid 19^{th} century, corrosion has become the largest long term problem for designers of reinforced concrete as it is the most important cause of concrete degradation [1]. Corrosion is also the most common reason for the need of repair when it comes to reinforced concrete (RC) [2]. Reinforced concrete degradation due to corrosion is expected to get worse as global temperatures and CO_2 concentrations increase in the coming decades the costs of maintenance will increase further to keep up with degradation [3] as bridges and infrastructure built in the during 20^{th} are moving towards the end of their service life. In the US this will lead to an increase of the annual spending of bridge repairs by 58% [4]. If repairs aren't kept up with the degree of degradation, not only will the costs pile up, but can also have catastrophic consequences with human lives at stake. A recent example where corrosion has been a driving factor in the total collapse of an RC structure is the Ponte Morandi Bridge in Genoa, Italy [5] in which 43 people lost their lives.

Steel is protected from corrosion due to the alkaline environment of the concrete. This protective environment can be damaged due to carbonation or chloride penetration [6]. Corrosion of the steel bars reduces the ultimate strength [7, 8] , and the ductility and the fatigue life of the reinforcement [9]. This can decrease the bending moment capacity of concrete members [10]. Furthermore volume expansion of corrosion products leads to splitting stresses of the concrete and creates cracks and spalling. Unfortunately, the corrosion levels in existing structures can not be measured directly, but the concrete cracks on the surface can be measured. Therefore, it is of high interest to gain further knowledge on the interconnection between corrosion damage and concrete cracks.

Previous research show a scatter in the effects cracks have on corrosion. Bending cracks have shown to have a significant impact on the loss of cross-sectional area of the reinforcement [11]. Furthermore, the width of the longitudinal cracks (corrosion induced cracks) are correlated with the amount of corrosion [12]. However [13] showed that as the longitudinal crack width increased, so did the pit volume, but determining local corrosion levels from this was challenging, as also shown by Berrocal et al [11]. If there was a method to accurately predict the corrosion of the reinforcement from the bending and longitudinal cracks, much would be gained in

terms of assesment and repair of RC structures. So, to understand how the cracks and corrosion influence each other, more research is needed. The combination of physical experiments with Finite Element Analysis (FEA) have the potential to increase our understanding of these effects. Previous research using FEA, modelled the effects of corrosion and the subsequent creation of cracks on a concrete with steel reinforcement [14, 15], but research is limited on the corrosion process under load and the full 3D effects a beam.

1.2 Aim

This thesis contributes to the overarching goal to quantify the corrosion damage through the measurement of the visible concrete cracks on the surface of concrete member. To achieve this, the following objectives were set up:

- Analyse available test results where crack pattern as well as corrosion characteristics have been carefully documented.
- Carry out 3D non-linear FE analyses of previously said tests.
- Compile and compare experimental and analysis results.
- Determine whether the 3D effects from pitting, corrosion, bending and splitting cracks can explain earlier experienced challenges in quantifying local corrosion damage based on measuring the visible cracks on the concrete cover.

1.3 Limitations

The limitations of this master's thesis works can be outlined as:

- The work in this master's thesis will be carried out through FEA and no experimental work will be carried out.
- This study will focus on a simply supported beam with a rectangular cross-section.

1.4 Methodology

A literature review was done to create a deeper understanding of how the corrosion influences the cracking behaviour of the concrete, and how the cracks in turn influence the propagation and distribution of the corrosion. Drawing from the work of previous researchers, results were compiled to compare the cracking behaviour and corrosion characteristics from the experiments with the FE analysis that was done using DIANA FEA 10.5. The effect of bending cracks was considered by a method of weakening the concrete elements. The swelling caused by the volume expansion of the corrosion products was modeled using interface elements between reinforcement and concrete and applied in time steps. The full 3D effects of the beam was considered.

2

Literature study

2.1 Corrosion and corrosion-induced cracks in Reinforced Concrete Structures

Corrosion is the primary cause of reinforced concrete degradation [1]. When exposed to air and water, steel undergoes chemical reactions such as corrosion [16]. However, in reinforced concrete structures, the steel is protected from corrosion by the concrete. This protection is due to the alkaline environment created by the concrete [6], which acts as a form of passive protection. Nevertheless, this protection can be compromised by carbonation or chloride penetration of the concrete cover [16]. Carbonation induced corrosion typically causes distributed corrosion on the steel (general or uniform corrosion), while chloride induced corrosion is more localized. Since chloride induced corrosion is localized, the corrosion tends to be more severe on a local level, reducing the cross-sectional area at a higher rate [6]. As the distribution of corrosion differs between carbonation and chlorides, chlorides affects the structural behavior and capacity more severely. Therefore, this thesis main focus is on the effects of chloride induced corrosion. The difference between pitting corrosion and general corrosion is shown in Figure 2.1

When steel undergoes corrosion, the resulting products occupy a larger space than the original steel, with ferric oxides being the primary byproduct [17]. Unfortunately for concrete, these oxidized products can occupy between 2 and 6 times the volume of uncorroded steel [17], and even up to 10 times when hydrated [16]. As a result, pressure is exerted on the surrounding concrete and tensile stresses are created, which leads to cracking of the concrete cover. These cracks will propagate along the length of the concrete [10, 18]. Figure 2.2 provides a good representation of the volume expansion and subsequent cracking of the concrete cover. The initiation and propagation of these cracks depend on several factors, such as the depth and porosity of the concrete cover, as well as the quality of the concrete (e.g., tensile strength) and the spacing and geometry of reinforcing bars. Additionally, the type of oxidized products created can also influence the crack formation [18]. Although these cracks are induced by corrosion, determining the amount of corrosion based on the crack width of these longitudinal cracks has been a challenge [11, 19].

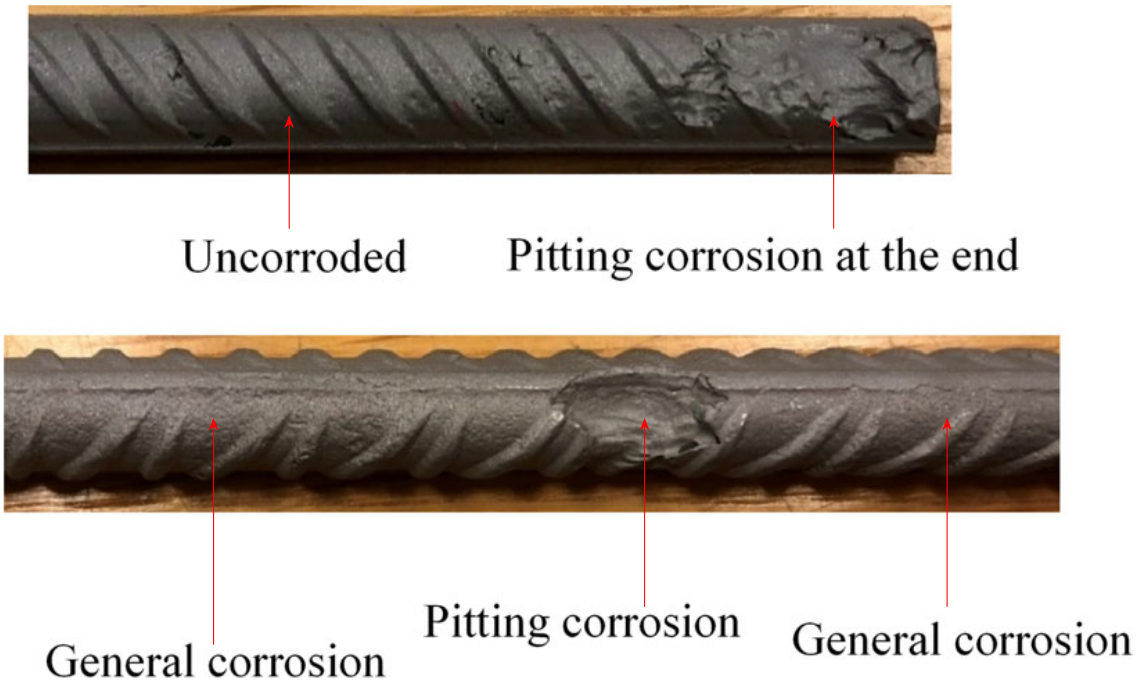

Figure 2.1: Pitting and general/uniform corrosion of a reinforcement steel bar used in concrete from [13].

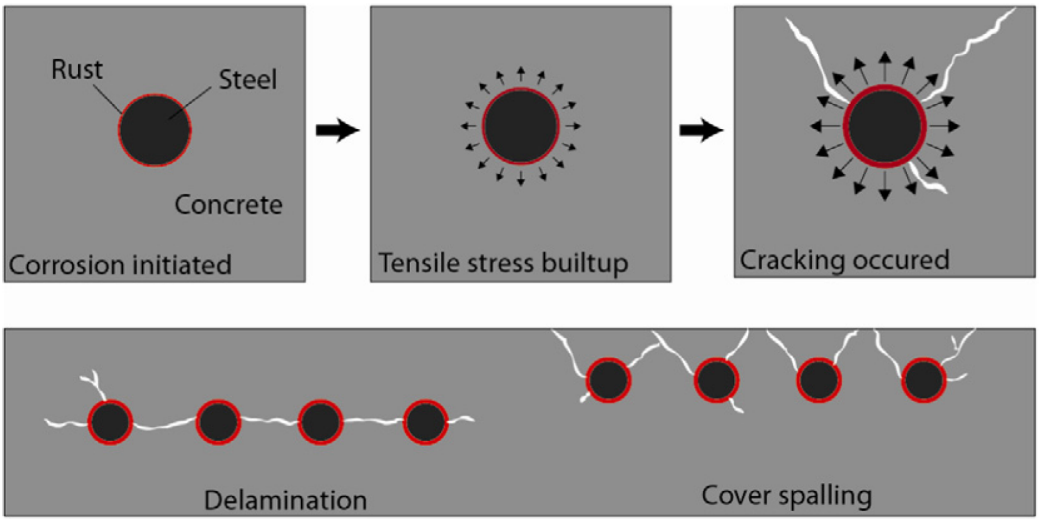

Figure 2.2: How corrosion-induced cracking causing concrete cover cracks and their cracking modes, from [18].

Corrosion of steel results in the replacement of its surface by corrosion products, leading to a loss of cross-section and a reduction in bond strength between the steel and concrete. At lower levels of corrosion, the ultimate bond strength may actually increase due to increased friction and limited options for the corrosion products to dissipate [20]. However, Almusallam et al. [20] demonstrated that, following the initial increase, a sharp decline in ultimate bond strength occurs after the first

corrosion-induced crack due to the formation of corrosion cracks around the reinforcement and this is mainly due to the loss of confinement of the reinforcement.

2.2 Interplay between bending cracks and corrosion-induced cracks

Cracks formed transversally to the reinforcement are primarily caused by bending or external restraints. These cracks provide direct access for chlorides to penetrate the concrete cover and reach the bars [17], leading to localized pitting corrosion. Previous research has established a cause-and-effect relationship between pitting corrosion and flexural cracks [11, 21, 13]. Additionally, as described previously, corrosion will cause longitudinal cracking of the concrete cover due to the accumulation of corrosion products [11, 13]. Chen et al. [13] showed that as the longitudinal crack width increased, so did the pit volume, but determining local corrosion levels from this was challenging, as also shown by Berrocal et al [11].

2.3 FEA of corrosion and cracking of reinforced concrete structures

FE modeling is commonly used to assess the structural integrity of both sound and corroded reinforced concrete (RC) structures [22, 23, 24, 25] and to analyze the effects of corrosion [14, 15]. While a simplified 2D model may suffice for many cases, the effects of corrosion are three-dimensional. Another important consideration is the interaction between the concrete and reinforcement, especially in the cases where cracking behaviour of the concrete is considered, therefore a bond-model need to be defined. Lundgren [26] developed a bond model for the effects of corrosion on the bond mechanism, which has since been improved [27].

Additionally, RC structures exhibit non-linear material responses, such as concrete cracking and reinforcement yielding [28]. While incorporating non-linear effects may increase calculation time, it is important to carefully consider which effects to include and which to disregard. Reinforcement is typically modeled with a stress-strain relationship that defines yielding, hardening, and rupturing. However, in situations where quasi-permanent loads with corrosion are applied, a simplified elastic model with Young's modulus may be sufficient for the reinforcement, if it is not expected to yield.

While uniform corrosion can be analyzed using a 2D model, localized corrosion due to chlorides requires a 3D model to accurately capture the effects [10]. When it comes to simulating the cracking of concrete, a smeared crack approach is commonly used in FE software, which can be further divided into fixed crack and rotating crack models. The rotating crack model is preferred as it aligns better with experimental results [28]. This model assumes that the average crack is always normal to the

direction of the maximum principal strain [29, 30]. The tensile curve developed by Hordijk [31] can be used to describe the tensile cracking in the FE model.

Previous research has demonstrated the effectiveness of simulating the effects of corrosion in a 3D environment [14, 32, 15]. However, these models are only pieces of a larger concrete structure. As a result, the analysis disregarded larger 3D-effects and imposed deformation. Wang et al. [15] modeled a fully 3D-beam and demonstrated the validity of using corrosion to induce cracks by comparing their simulation results to experimental data. This study also emphasized the significance of including stirrups in the model, as they greatly affect the formation of cracks due to corrosion. In Echen et al.'s study [14], the load was applied after corrosion as a pull out of the bar, and the subsequent cracking was also not applied on top of the member but in the longitudinal direction of the thin section. In Wang et al.'s study [15], no external loading outside of the corrosion was considered. In a real situation loads would be applied prior to long-term corrosion effects, and cracking would occur subsequently. Therefore, incorporating load or imposed deformation in the model would better represent real-world situations. Thus, to better simulate real-world scenarios, it is important to analyze the effects of corrosion on concrete cracking on a full 3D structure after imposed deformation or external loading has been applied. If not, one would assume that load and transversal cracks have no effect on corrosion and corrosion-induced cracks. Tahershamsi et. al. [33] showed that the load application together with the corrosion process could be modeled together as well as showing good correlation between crack pattern of the FE analysis and experimental results.

2.4 Corrosion and bond models

In order to replicate the consequences of corrosion in a simulated environment, it is essential to accurately capture the real-world effects and behavior. A relevant model was developed by Lundgren [26], which is implemented for 3D Finite Element Analysis (FEA). This model is designed for use in the DIANA FE program, in analyses where both the reinforcement and concrete are modeled with 3D elements. With this modelling method, it is possible to simulate how the volume expansion of corrosion products exerts pressure on the surrounding concrete, leading to concrete cracking.

2.4.1 Interface elements

The corrosion model takes advantage of the interface elements that establish the relationship between the relative displacement $\mathbf{u}$ and the traction $\mathbf{t}$ at the interface of 3D elements, namely the concrete and reinforcement. The interface models describes both the corrosion and the bond, with two separate models divided into two distinct layers surrounding the reinforcement. Thus, the corrosion and bond model are integrated into a single interface element for ease of use. Figure [2.3] provides a visual representation of the interface elements used in the model.

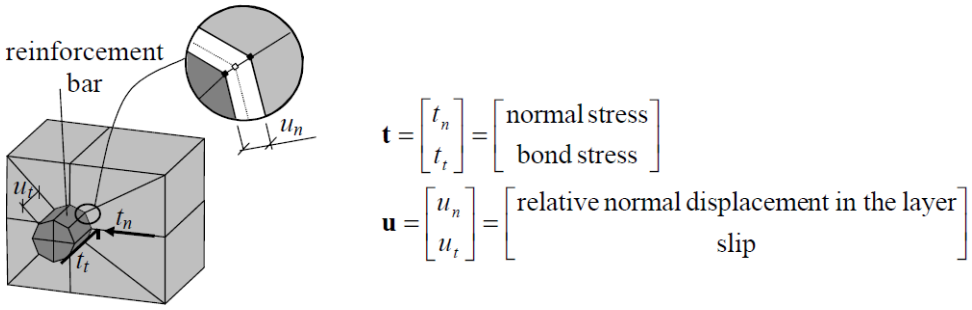

Figure 2.3: Physical interpretation of the the variables in the interface elements from Lundgren [26].

2.4.2 Corrosion model

The corrosion model incorporates the volume expansion of corrosion as a layer that expands in proportion to the amount of steel that has corroded. The extent of this expansion is dependent on the type of corrosion products formed, and is usually modelled as 2.0. As explained earlier, different corrosion products can varying degrees of volume expansion. In our analysis 2.0 will be seen as a reference point where the volume expansion will be changed to see the effects of such a change. The distance x represents the depth of penetration of the corrosion into the cross section of the steel bar. The "free increase" in radius, denoted by **a**, is the radius at which no normal stresses would be present. However, due to the resistance from the surrounding concrete, the actual increase in radius, referred to as u_{ncor}, is smaller. This creates a strain in the rust, from which the normal stresses are then determined.

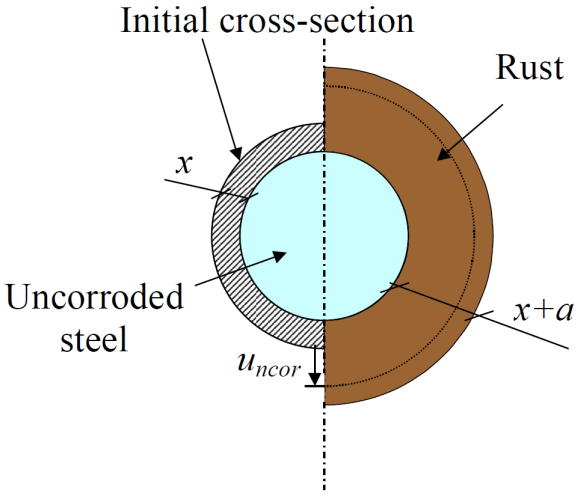

Figure 2.4: Physical interpretation of the variables in the corrosion model from Lundgren [26].

2.4.3 Bond model

The bond model represents the frictional behavior of the interface between the rebars and concrete using elasto-plastic theory to account for stresses and deformations. It simulates the adhesion and mechanical interlocking that occur in the real world. Specifically, the model describes the stresses and deformations of the bond layer of the interface element surrounding the reinforcement. Two yield functions are used in the model: F_1, which assumes that adhesion is negligible, and F_2, which represents the upper limit of a pull-out failure. A visual representation of these yield functions is presented in figure [2.5]. The variables μ and c in the yield functions of F_1 and F_2, respectively, are further explained in Lundgren 2001 [26].

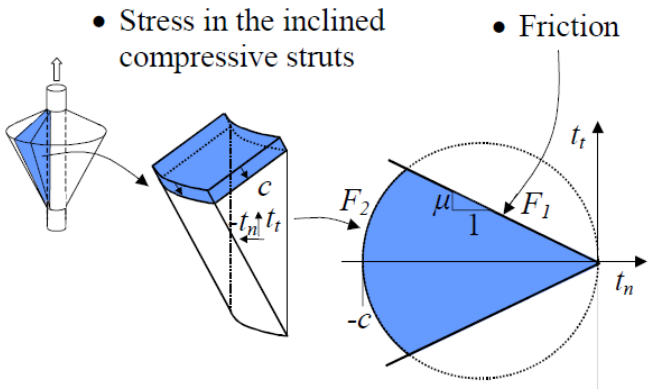

Figure 2.5: Yield surface of the bond model from Lundgren [26].

2.5 Discussion

Previous studies have highlighted the difficulty in establishing a connection between concrete flexural cracks, corrosion, and the resulting corrosion-induced cracks. Researchers have attempted to address this issue through experiments designed to measure the effects of reinforcement corrosion on concrete cracking [21, 14, 11]. While 3D analyses have been conducted to investigate the effects of corrosion on thin concrete sections [14] and 3D RC beams [15], there is a notable gap in the literature where no analyses have been conducted to explore the combined effects of corrosion, 3D behavior, and external loading. The aim of this thesis is to investigate the 3D effects of pitting corrosion, flexural, and longitudinal cracks, and to compare the FEA analysis results with those of previous researched by Berrocal et al. [11].

3
Experiment

The experiments used as benchmarks were conducted by Berrocal et. al. [11] where they studied the effects of corrosion on the cracking behaviour of a reinforced concrete beam under imposed deformation. This chapter presents the major aspects of this experiment.

3.1 Geometry and material properties of the beam

The beam used in the experiment had a length of 3 meters, a height of 250 millimeters, and a width of 200 millimeters. The concrete had a water-to-cement ratio of 0.45. The reinforcement consisted of longitudinal tensile reinforcement of ⌀16 millimeters (bottom) and ⌀10 millimeters for the compressive reinforcement (top). Additionally, closed loop stirrups with a spacing of 200 millimeters and ⌀8 millimeters were added. The reinforcement was cast with a concrete cover of 20 millimeters.

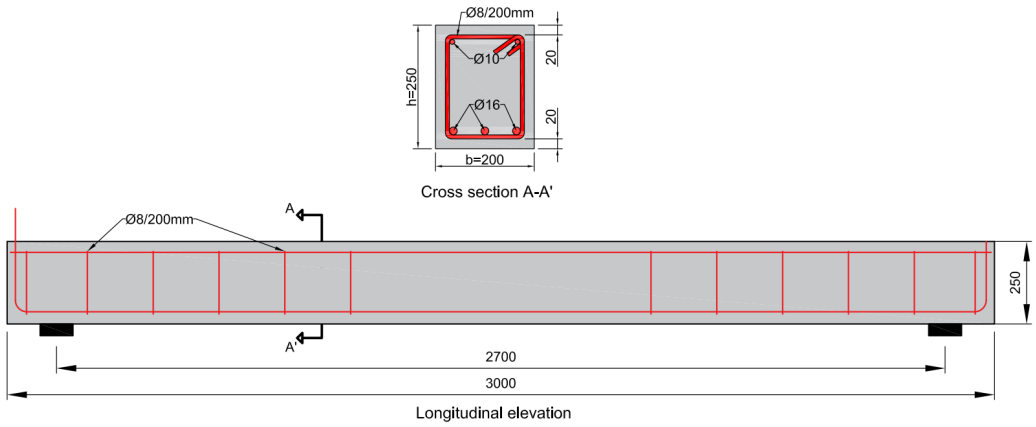

Figure 3.1: Beam Geometry and cross-section [11].

The compressive strength of the concrete was tested in accordance with [34], where three 150-millimeter cubes were tested in a compressive test, resulting in a compressive strength of 68.2 MPa (CoV = 5.6%) at 28 days. The rest of the material properties were derived from the compressive strength using the fib model code [35], and are presented in Table 4.2. The reinforcement was made of strength B500B with a yield strength of 500 MPa.

3.2 Pre-cracking and accelerated corrosion process

A four point bending test was conducted to induce transversal crack prior to the corrosion process. The load was applied in two load cycles of 60 kN to produce the intended cracks. These cracks are needed to allow for the chlorides to penetrate the concrete cover and to induce pitting corrosion. After the beam was subjected to a constant deformation by connecting it upside down to an identical beam using a clamping device and threaded bolts, as shown in Figure 3.2. The complete loading procedure is explained in more detail in Berrocal et al. [11]. This imposed deformation was sustained for 96 days before the accelerated corrosion process was initiated with an impressed current.

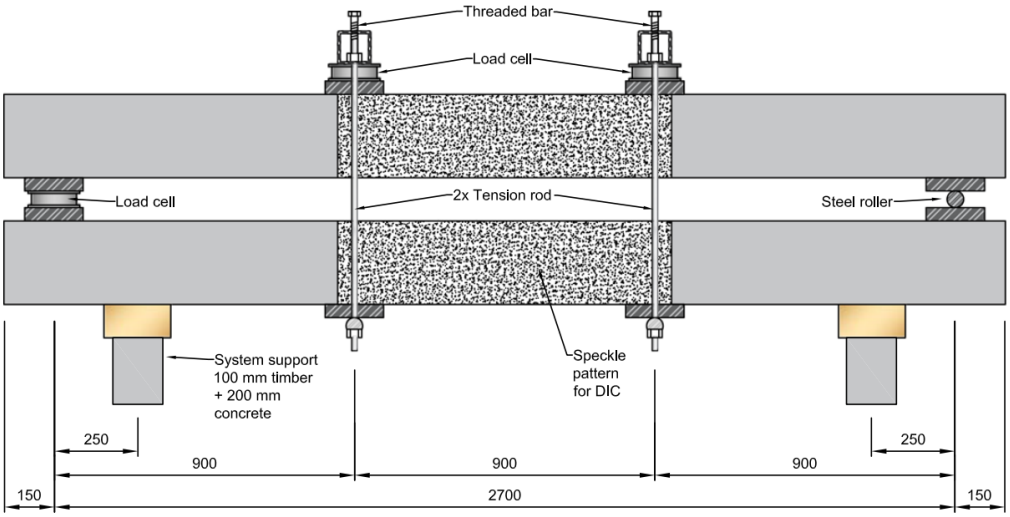

Figure 3.2: Loading setup of the experiment [11].

To simulate the non-uniform distribution of chloride-induced corrosion, sodium chloride solution transport fibers were placed in the upper-middle part of the beam. The tensile reinforcement was connected to a positive DC power source, while the negative source was connected to the copper mesh cathode. This procedure, which is illustrated in Figure 3.5, allowed for the artificial corrosion of the beam. For a detailed description of the setup, refer to Berrocal et al. [11]. After the accelerated corrosion test was completed, the concrete cover was removed, cleaned, and the corrosion levels were measured using 3D scanning.

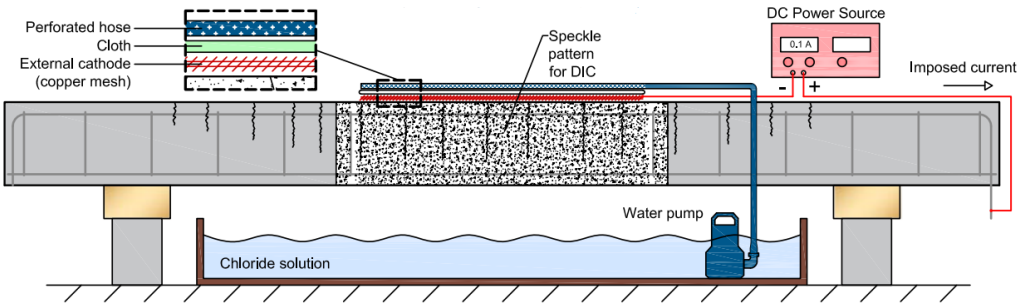

Figure 3.3: Corrosion setup of the experiment [11].

To measure the crack width of the bending cracks, a distributed optical fiber sensor (DOFS) setup was implemented. This method does not measure the crack width directly, but the strain along the fiber sensor. This method was also used to measure the longitudinal cracks on the tensile side of the beam. The DOFS setup is shown in Figure 3.4.

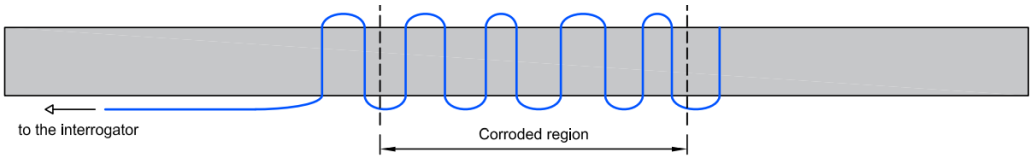

Figure 3.4: DOFS setup on the tensile side of the beam [11].

Digital Image Correlation (DIC) system was used to document the crack pattern and maximum crack width during the pre-cracking procedure, as well as monitor the initiation and propagation of corrosion-induced cracks during the accelerated corrosion phase. DIC is a used for monitoring the formation and growth of cracks in concrete due to its ability to track 2D strain fields on the surface of an object over time. A sort of virtual DIC measurement will be used to measure the crack widths of the FE model as well, and will be explained more in detail in the next chapter.

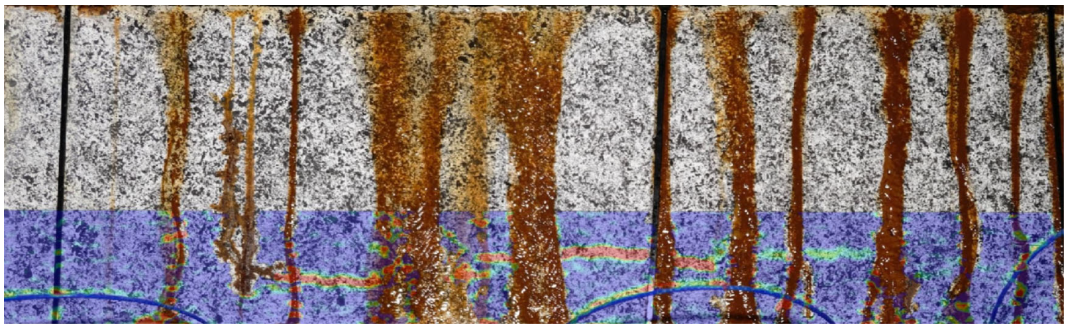

Figure 3.5: DIC vertical strain field of the experiment [11].

4

FEA Analysis and interface/corrosion model

The tested beam in [11] was studied using the computer software DIANA FEA in a NLFEA 3D model. The beam in question was modelled to investigate if the corrosion model can accurately predict the crack widths and cracking behaviour of a beam under imposed deformation with effects of corrosion being applied over time. Multiple analyses was done with varying distributions of the measured corrosion in the experiment and altering the volume expansion in the corrosion model. The beam and tensile reinforcement was modelled with 3D solid continuum elements. The reinforcement were modelled as polygonal sheet with 8 sides which where extruded into the beam which thereby replaced the original beam material. The stirrups and compressive reinforcement were both modelled as embedded reinforcement. To simulate how the tensile reinforcement corrodes and expands due to the formation of corrosion products the implementation of the corrosion model created by Lundgren [26] was used. The corrosion model is implemented using interface elements between the steel and the concrete surfaces.

4.1 Design of FE models

First we want to determine if the FEA model can reproduce the crack pattern and crack widths of the beam tested in Berrocal et. al. [11]. Secondly, if the model shows similar crack pattern and crack widths as the experiment, we want to know what is the main influencing factor of the crack pattern and crack widths and crack propagation of the FE model. The aim of the analysis is therefore not made to reproduce the exact crack widths as measured in the experiment, rather on the governing factors influencing the crack pattern and crack widths in order to better understand how the crack pattern of the experiment emerged. In the Figure 4.1 the parameters are presented. The beam geometry was kept constant as there was only experimental data from one beam compared with. The pit locations and material properties are kept constant for this reason as well. The volume expansion was altered to study the effects it would have one the crack pattern and crack widths of the concrete cover as different corrosion products can have different degrees of volume expansion. Secondly, to study the effects different corrosion distributions to see their effects on crack pattern and crack widths.

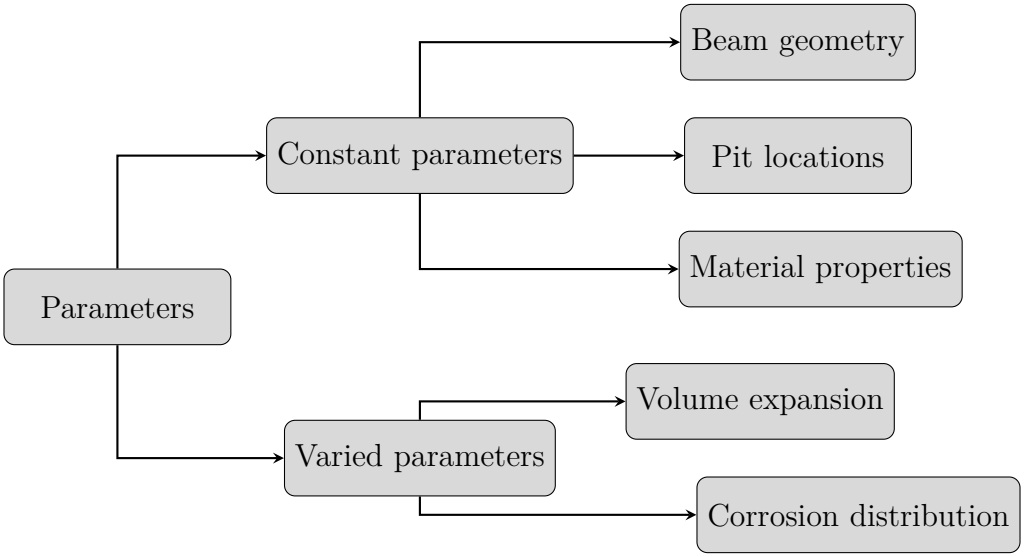

Figure 4.1: Flow chart of the parameters that were constant during the analysis and those that were changed to better understand the factors governing crack pattern and crack widths.

4.2 Overview of FE models

The FE models that were modelled and analyzed in DIANA 10.5 are presented in Table 4.1 where the name, the chosen corrosion distribution and the volume expansion is presented. The first corrosion distribution are chosen as to mimic the corrosion found on the reinforcement in the experiment. Second corrosion distribution is where the corrosion was applied as an average corrosion over the corroded region. Third and last is where there is no corrosion applied at the pits. This is to simulate the effects of where the corrosion products dissipate through the bending cracks and therefore does not apply any stresses to the surrounding concrete. The third analysis was not incuded which used a volume expansion of 1.5, this was however removed from the results as no corrosion induced cracks formed.

Table 4.1: Overview of FE models

FEA Model	Corrosion distribution	Volume expansion
PU1_FEA	Pitting and uniform	2.0
U1_FEA	Uniform	2.0
UO1_FEA	Uniform, no corrosion at pits	2.0
PU2_FEA	Pitting and uniform	2.5
U2_FEA	Uniform	2.5
UO2_FEA	Uniform, no corrosion at pits	2.5
PU4_FEA	Pitting and uniform	1.8
U4_FEA	Uniform	1.8
UO4_FEA	Uniform, no corrosion at pits	1.8
PU5_FEA	Pitting and uniform	1.9
U5_FEA	Uniform	1.9
UO5_FEA	Uniform, no corrosion at pits	1.9

4.3 Beam geometry

Analyzing a complete beam using small elements can be time-consuming and computationally intensive. Therefore, a symmetry line along the beams longitudinal direction was created. This symmetry line is presented in Figure 4.4. The beam geometry and the support conditions chosen is presented in Figure 4.2 and the geometry with the concrete beam hidden to expose the reinforcement and weakened elements geometry shown can be observed in Figure 4.3.

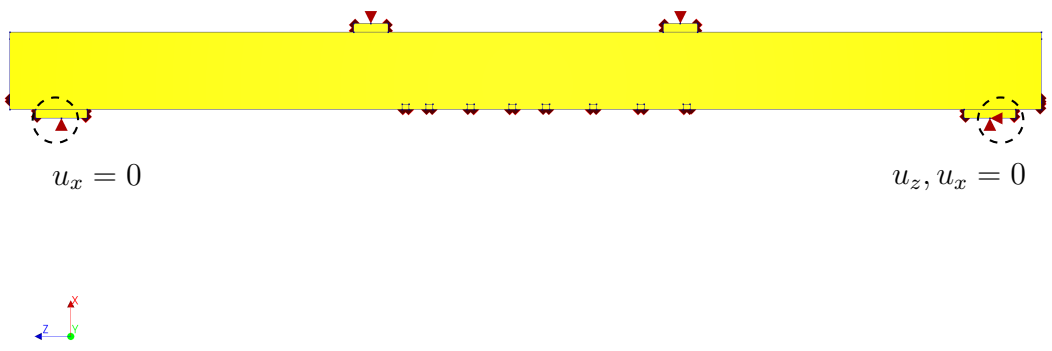

Figure 4.2: 3D view of the beam with support conditions.

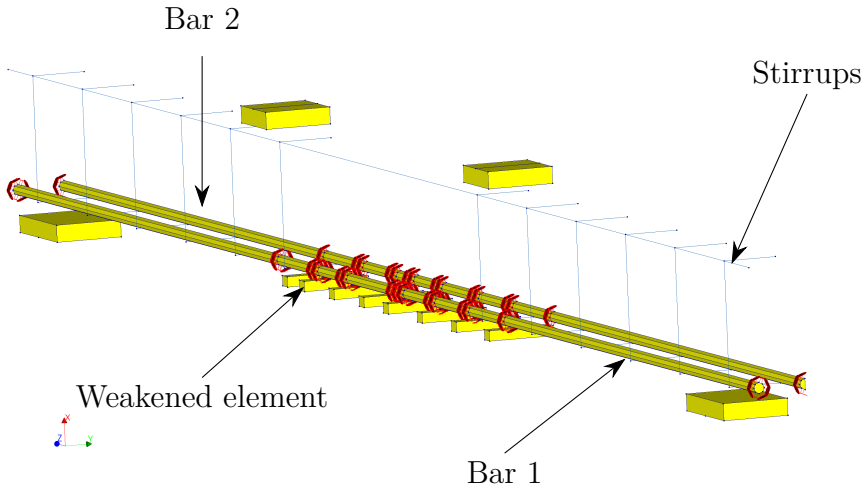

Figure 4.3: 3D view of the beam with stirrups and 3D reinforcement showing as well as the weakened elements.

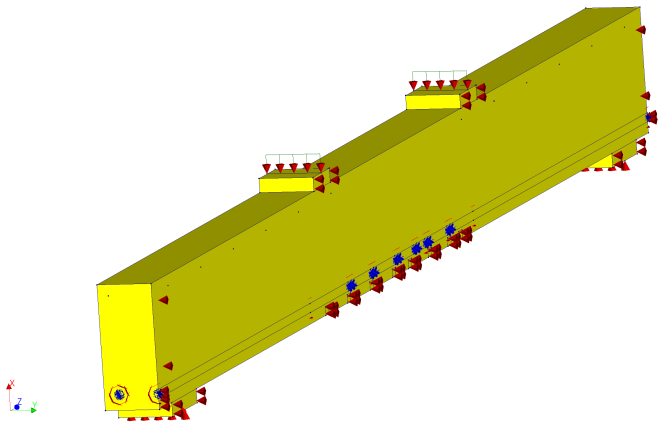

Figure 4.4: 3D view of the beam showing the backside of the beam and symmetry line

4.4 Material model for concrete

The material properties for the concrete used in the FEA can be observed in Table 4.2. The compressive strength of concrete was retrieved from the compression tests conducted by Berrocal et. al. [11]. With the compression strength known the rest of the material properties was retrieved from the fib model 2010 [35]. All of these inputs are presented in Table 4.2. With the tensile strength given, the tensile strength-strain relationship by Hordijk was used [31].

Table 4.2: Material properties for concrete elements

Material property		Value	
Mean compressive strength [11], [36]	$f_{cm} = f_{ck} + 8$ [MPa]	58	[GPa]
Mean tensile strength [36]	$f_{ctm} = 2.12 \cdot ln(1 + \frac{f_{cm}}{10})$	4.07	[MPa]
Tensile fracture energy [35]	G_f	103	[N/m]
Modulus of elasticity [36]	$E_{cm} = 22 \cdot (\frac{f_{cm}}{10})^{0.3}$	37	[GPa]

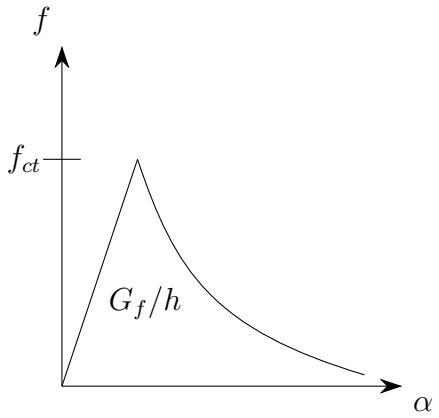

Figure 4.5: Tensile stress strain curve propsed by Hordijk [31]

4.5 Material model for reinforcement

The reinforcement is modelled in two different ways. The stirrups and compressive reinforcement are modelled as embedded reinforcement. The tensile reinforcement in the bottom are modelled as solid 3D elements. The reinforcement are modelled as in the experiment as steel with a Young's modulus of 210 GPa. The steel used in the experiment was of reinforcement type B500B which equals a yield strength of 500 MPa, this was however not needed as the steel is never supposed to yield during the experiment or the FEA. Since the experiment was studying the effects of chloride induced corrosion, which is a localized type of corrosion, a distinction must be made in the FEA between different sections of the tensile reinforcement, depending on the measured corrosion at each section. How this is done is presented more in depth later in this chapter.

4.6 Loading and support plates

The loading and support plates were modeled as steel plates. These are used to prevent stress concentrations so that there aren't any unwanted effects such as cracking and failure of the material around the application of imposed deformation. The steel plates had an elastic modulus of 210 GPa and a Poission's ratio of 0.3.

4.7 Weakened elements

To simulate the creation of the bending cracks which the beam in Berrocal et. al. [11] experienced during the pre-loading phase, a kind of weakened element was implemented. These weakened elements were placed at the origin of the cracks from Berrocal et. al. [11] just so that these would trigger the formation of cracks when the imposed deformation was applied. These weakened elements were modified to be the 5% weakest fractile of elements with regards to the measured compressive strength measured by Berrocal et. al. which results in a mean compressive strength of 55 MPa. From this the rest of material properties can be determined are presented in 4.3

Table 4.3: Material properties for weakened elements

Material property		Value	
Mean Compressive strength [36]	$f_{cm} = f_{ck} + 8$	55	[GPa]
Tensile strength [36]	$f_{ctm} = 2.12 \cdot ln(1 + \frac{f_{cm}}{10})$	3.84	[MPa]
Tensile fracture energy [35]	G_f	97	[N/m]
Modulus of elasticity [36]	$E_{cm} = 22 \cdot (\frac{f_{cm}}{10})^{0.3}$	37	[GPa]

4.8 Corrosion

In this thesis, the effects of corrosion on the crack pattern and crack widths are investigated. In the experiment in which the FE-analysis is based on, there are two types of corrosion present. Pitting corrosion and uniform/general corrosion. The pitting corrosion are sections with high amounts of corrosion and uniform the parts in between the pits which have much lower amounts of corrosion and are spread over a larger area. These different levels of corrosion needs to be distinguished in the FE-analysis. To create sections with different amounts of corrosion, dividing the reinforcement bars into different sections is needed. The pit length in the FE model is chosen to be equal to the element size of the model, the location of each pit is then retrieved from the data provided in Berrocal et al. [11]. The pits are therefore measured from the peak of the pit and 10 mm in both directions. All the areas that are not part of the pitting corrosion are referred to as uniform corrosion sections and like the pits are assigned the average corrosion depth of that area. All regions outside of the corroded region are supplied with the same type of interface elements, but instead the corrosion depth are assigned as 0. The distinction between these areas in the FE model are presented in Figure 4.6.

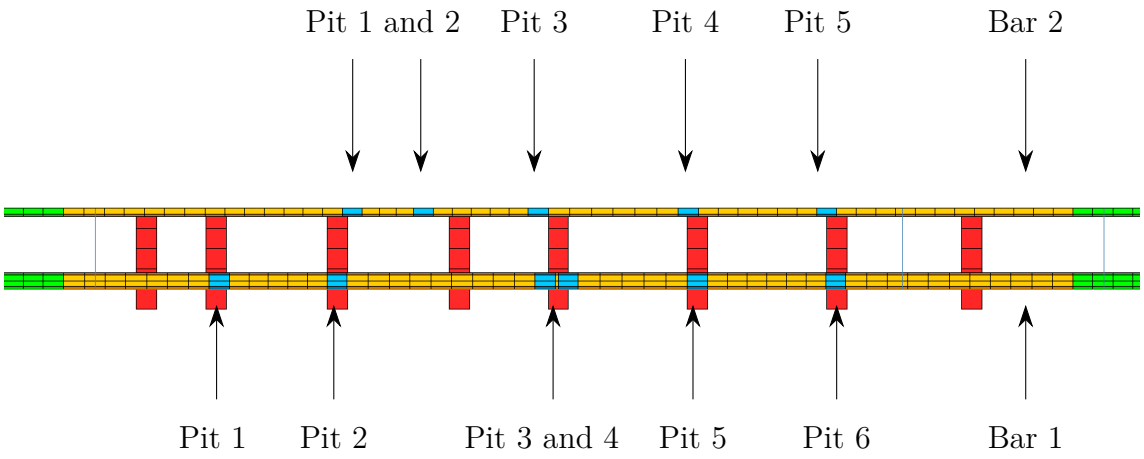

Figure 4.6: 3D view of the reference beam with the location of each pit, orange color is the corresponding uniform corrosion areas and green where no corrosion takes place. Red element are the weakened elements where the pre-loading cracks are produced.

To determine the corresponding corrosion at each section, the corrosion depth needs to be calculated. In the data provided by Berrocal et. al [11] the original cross-section A_o and the measured corroded cross-section A_c are provided. The corrosion depth over Bar 1 and Bar 2 is presented in Figure 4.7 and 4.8 respectively as well as the location of sections with pitting corrosion.

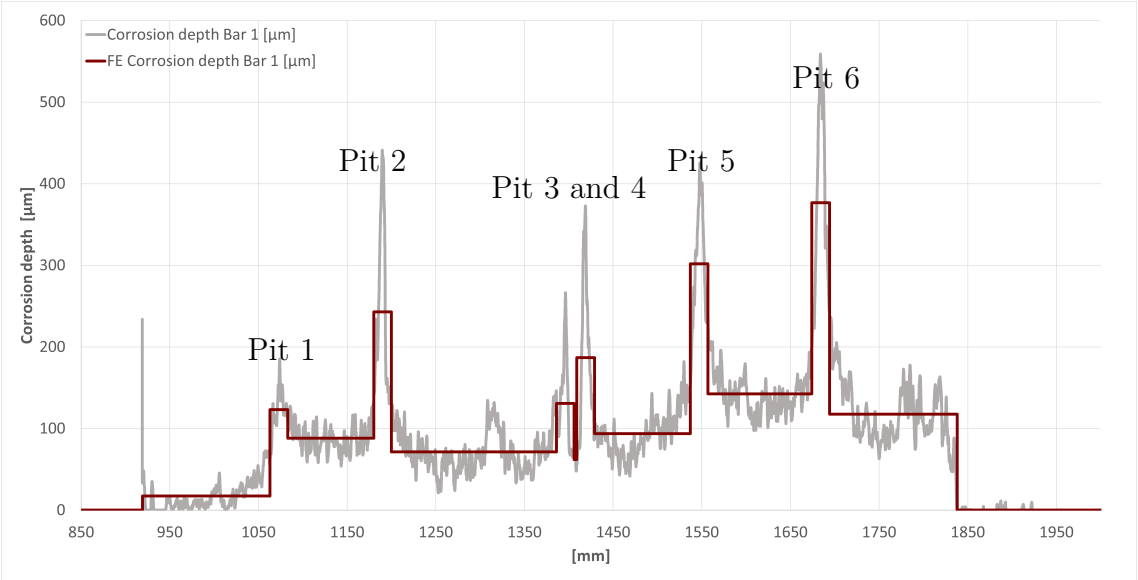

Figure 4.7: Cross sectional loss of Bar 1 and the corresponding corrosion depth for the FE analysis.

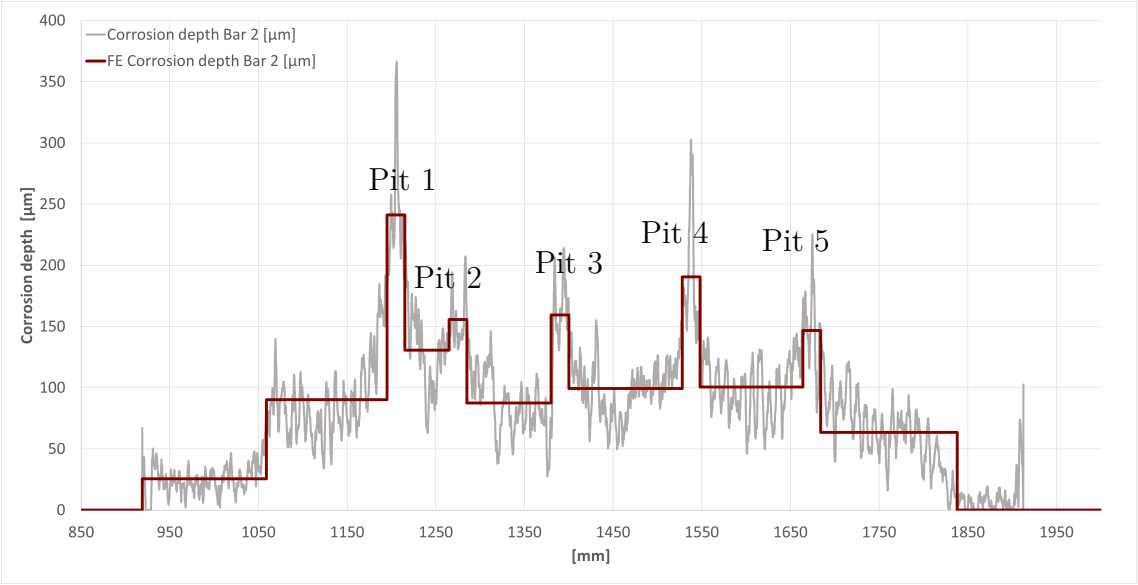

Figure 4.8: Cross sectional loss of Bar 2 and the corresponding corrosion depth for the FE analysis.

The corrosion depth which was used as input to the corrosion model was determined by dividing the corroded cross section A_c with the original cross section after corrosion A_o, we get the loss of cross-sectional area $C_{\%}$. Given the average $C_{\%}$ over each section, with the radius of the original cross section r_o the corrosion depth x can be determined. The formulas for calculating the corrosion depth are presented in the following mathematical expressions:

$$C_{\%} = \frac{A_c}{A_o}$$

$$r_0 = \sqrt{\frac{A_o}{\pi}}$$

$$x = r_0 - \sqrt{C_{\%}} \cdot r_0$$

4.9 Concrete-reinforcement interface

The concrete and reinforcement interaction were modelled with special interfaces developed by Lundgren [26], and was applied as a user supplied subroutine in the DIANA FE program. The corrosion are applied as an expansion of the interface layer between the reinforcement and concrete. This model was calibrated improved later on and in this analysis the calibration are as presented in [10]. During loading, the mechanical behaviour of the rust is described by the power law $\sigma_n = K_{corr} + \varepsilon^p_{corr}$ which simulates how the stiffness of the corrosion products increase as stresses increase. $K_{corr} = 14$ GPa and $\varepsilon^p_{corr} = 7.0$ as calibrated by Lundgren [10]. Corrosion depth input for Bar 1 and 2 in Table 4.5 and 4.6 respectively. Interface stiffness that are connected to bond model of the reinforcement are presented in Table 4.4. DSSX and DSSY represent the shear stiffness in the x and y-direction and DSNZ are the interface normal stiffness along the Z direction.

Table 4.4: Interface stiffnesses of the bond model

DSSX $[N/m^2]$	DSSY $[N/m^2]$	DSNZ $[N/m^2]$
$35 \cdot 10^6$	$35 \cdot 10^6$	$350 \cdot 10^6$

The corrosion model works in such a way that the corrosion depth x increased with each time step in the FE analysis. With the volume expansion given, the free increase a as is presented in figure 2.4 can be calculated by:

$$a = \sqrt{r^2 + (v-1) \cdot (2rx - x^2)} - r$$

The increase is however constrained by the surrounding concrete, resulting in the reduced displacement u_{ncor} and the subsequent compressive radial stresses and tensile hoop stresses causing the concrete to crack. The corrosion model are imported as a material applied in the interfaces which the subroutine then uses to simulate and apply the volume expansion of the corrosion which then creates stresses and tensile hoop stresses on the concrete. The concrete compressive strength are chosen to be the same as the concrete material property as in Table 4.2 and the radius of the rebar are the radius of the tensile rebars used in Berrocal et. al. [11]. The corrosion penetration depth that were used in the corrosion model is presented in Table 4.5 and 4.6. The volume expansion of the rust was varied in the analyses but also the original volume expansion of 2.0 was used as suggested in Lundgren 2001, [26] to study the effects of increased or decreased volume expansion.

Table 4.5: Corrosion depths for Bar 1

Section	Uniform corrosion	Pitting corrosion	
1	17	123	[μm]
2	88	242	[μm]
3	71	131	[μm]
4	62	187	[μm]
5	94	302	[μm]
6	143	377	[μm]
7	117	-	[μm]
Average corrosion	104	-	[μm]

Table 4.6: Corrosion depths for Bar 2

Section	Uniform corrosion	Pitting corrosion	
1	25	-	[μm]
2	90	241	[μm]
3	131	156	[μm]
4	87	159	[μm]
5	99	191	[μm]
6	101	147	[μm]
7	63	-	[μm]
Average corrosion	150	-	[μm]

4.10 FE mesh

The beam and tensile reinforcement was modelled using 3D solid continuum elements: Bricks CHX60, pyramid CPY39, tetrahedron CTE30, wedge CTP45. The elements used quadratic interpolation and gauss integration. For the interface elements between the tensile reinforcement and concrete the two planed CQ48I elements were used. The size of the elements are recommended from [37] to be no larger than the following $(\frac{l}{50}, \frac{h}{6}, \frac{b}{6})$, this equals to a size of 60 37.5 and 33 mm. With a split of the beam along the symmetry line this would instead equal 16 mm. The final element size was however chosen as 20 mm to match the length of the pits observed the experiment by Berrocal et. al. [11].

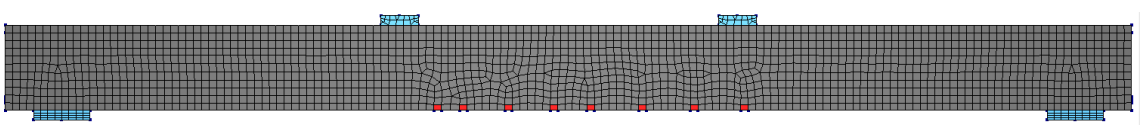

Figure 4.9: 3D FE Mesh of the reference beam with grey elements are the regular beam elements, blue load and support plates, and red the weakened elements.

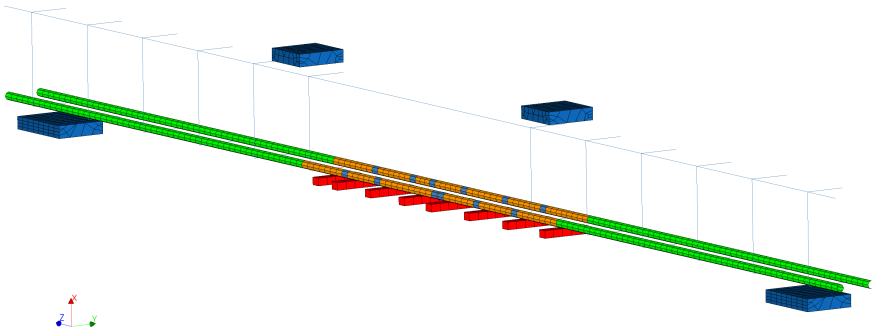

Figure 4.10: 3D FE Mesh of the reference beam with the reinforcement bars, stirrups and weakened elements shown.

4.11 Load increment and convergence criteria

The imposed deformation was applied on the beam at the middle of the load plates. This was done to induce the cracks needed for the corrosion to start due to chloride penetration. The deformation was imposed in steps with an increase of 0.2 mm of deformation in 10 steps, and then 0.4mm in 9 steps which produced a deformation in the middle of the beam of 6.6 mm which corresponds to the deformation of the first load cycle in the experiment that was measured as 6.6 mm. After the imposed deformation phase, the corrosion part of the analysis was started. This was done by applying the aforementioned corrosion model developed by Lundgren [26] in time steps. Time steps are applied in 100 steps where the corrosion are applied as $1/100^{th}$ of the final corrosion depth in micrometer at each time step. The chosen iteration method was Newton-Raphson for the pre-loading and for the corrosion time steps a secant iteration, (quasi-Newton iteration) with BFGS (Broyden, Fletcher, Goldfarb, and Shanno) method. The maximum number of iterations for both the imposed deformation as well the corrosion was set as 50. Imposed deformation was iterated until convergence, but for convergence to occur for the corrosion analysis it could take hours for a time step to finish, and was therefore limited to 50 iterations. For the tolerance limits of energy, displacement and force norm was chosen 0.0001, 0.01 and 0.01 respectively.

5

NLFEA Results

In this chapter, the results from the Finite Element analysis are presented and compared with test results of the experiment done by Berrocal et. al. [11]. First the results from the imposed deformation will be presented, and how the weakened elements help with producing the bending cracks at the locations in which they appeared in the experiment. Second, the analyses of PU_FEA, U_FEA and UO_FEA with the initiation of cracks, final crack pattern and the measured crack widths are presented and compared with the results of the experiment. Lastly, the effects of varying the volume expansion and the growth of cracks over time are presented.

5.1 Bending cracks

Overall the method of introducing the weakened elements at the location of the bending cracks as observed in the experiment show good results. Bending cracks formed at all weakened elements but 1. The bending cracks measured in the FE analysis is compared with those of the experiment and is presented in table 5.1. As can be observed in table 5.1 the bending cracks differ to an extent were the bending bending cracks was overall larger for the FE analysis where they formed. They are however in the same range as is therefore acceptable for the purpose of the analysis of corrosion-induced cracks.

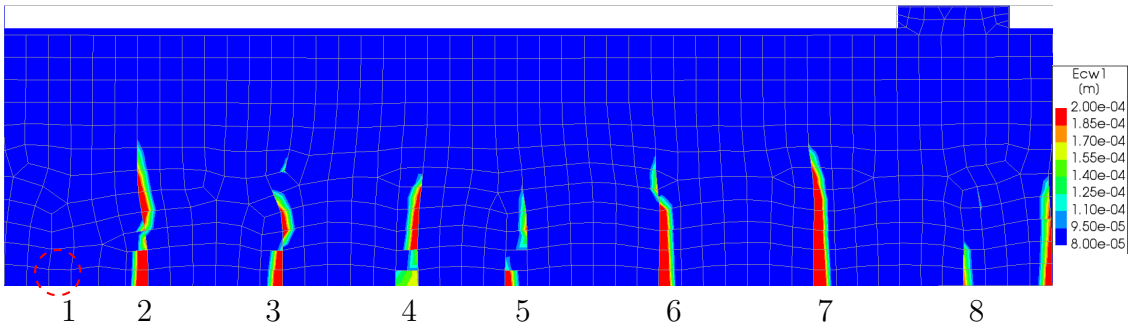

Figure 5.1: Crack pattern after applying imposed deformation with numbering of the bending cracks. Red ring indicate the location of the weakened element where a bending crack did not form.

Table 5.1: Measured crack widths of the bending cracks in both FE analysis and experiment.

Bending crack	Crack width [mm] (FEA)	Crack width [mm] (Experiment)
1	0.04	0.13
2	0.21	0.10
3	0.16	0.14
4	0.16	0.10
5	0.13	0.14
6	0.19	0.15
7	0.22	0.14
8	0.09	0.17

5.2 PU1_FEA

In this analysis the corrosion distribution was modelled as close as what was measured on the reinforcement after the experiment. The crack patterns are presented in figure 5.2 and show good correlation with the crack pattern of the experiment. The crack initiation occurs both between the bending cracks and at the bending cracks, which corresponds to the location of pitting corrosion. The overall final crack pattern show a good correlation with the crack pattern of the experiment on the lateral side. Cracking of the tensile side is more or less absent except for some cracking between the 7^{th} and 8^{th} bending crack. This agrees well with the experimental results as only minor cracks occurred on the tensile side.

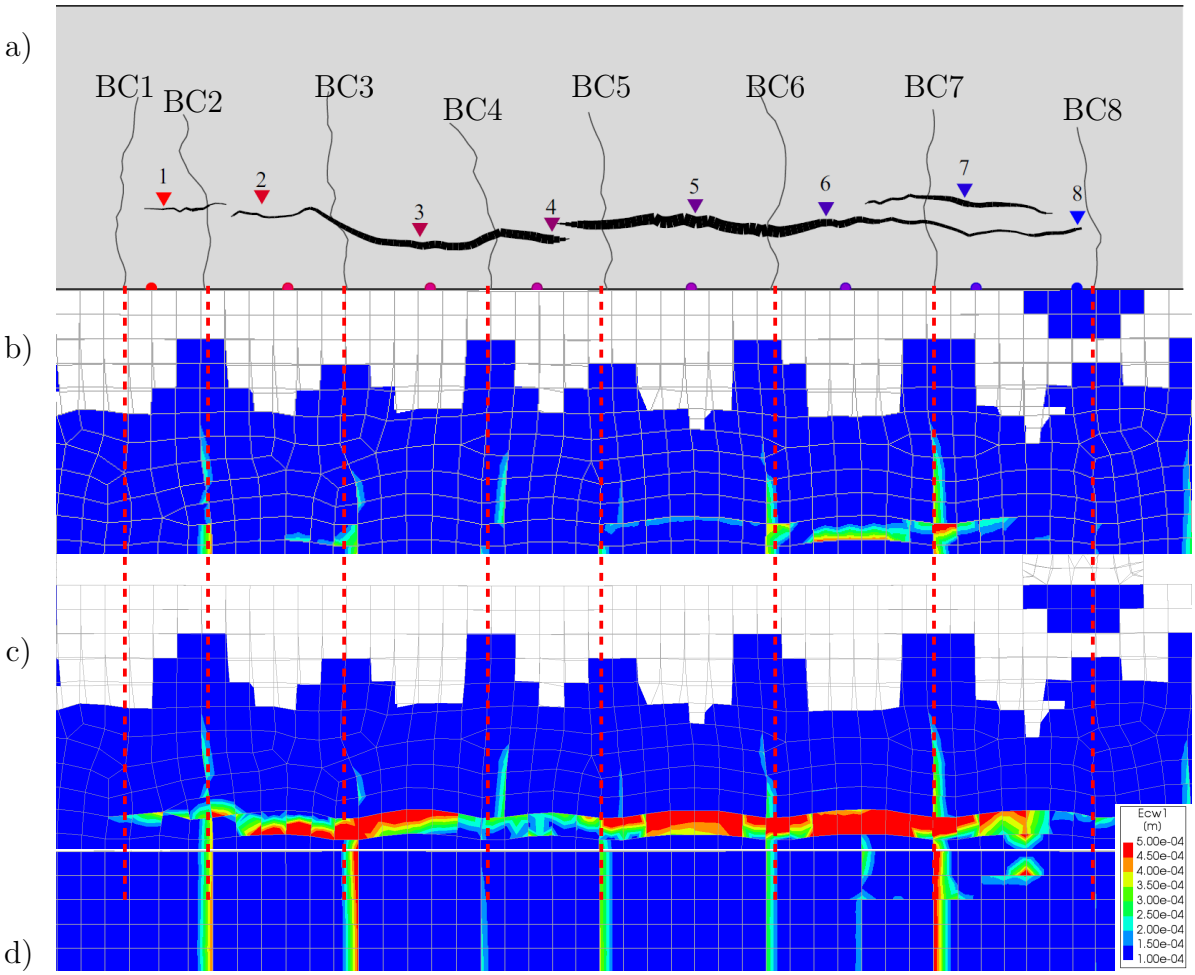

Figure 5.2: a) The recreated final crack pattern of the experiment. b) The crack pattern of the analysis after half the time has passed. c) and d) Represent the lateral and tensile side crack patterns at the end of the FE analysis. The numbers at the top of the image represent the numbering of the bending cracks. The triangles are where the experiment measured the crack widths with regards to time in the experiment, and dots where the crack widths of the tensile side was measured with regards to time.

To study the effects of the corrosion distribution, the corrosion distribution along with the final crack widths of the corroded region were plotted in the same graph and are presented in figure 5.3. What can be seen is that there is no clear correlation between the local corrosion levels and the longitudinal crack widths in the same section. As the location with the highest pitting corrosion of bar 1 does not show the highest crack widths on the lateral side. The maximum crack widths is somewhat offset to the left of the highest amount of corrosion. This is the location of the highest uniform corrosion on bar 1. Suggesting that the uniform corrosion and pitting corrosion close to this point is causing the point of maximum crack width. A significant drop in crack widths appear around position 1450mm from the left side of the beam, which shows the lowest uniform corrosion of Bar 1 and the area with with no pitting corrosion relatively near compared to other areas. The shape of the

crack width distributions also show no resemblance with the ones measured in the experiment as can be observed in 5.4.

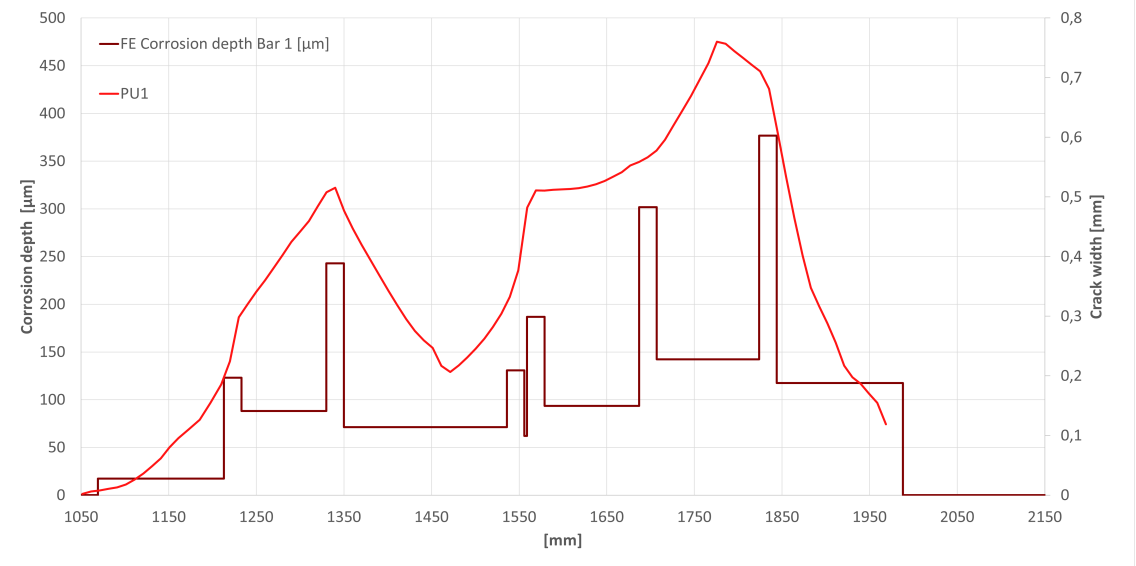

Figure 5.3: Comparison between the crack width and the corrosion distribution of Bar 1 of PU1_FEA.

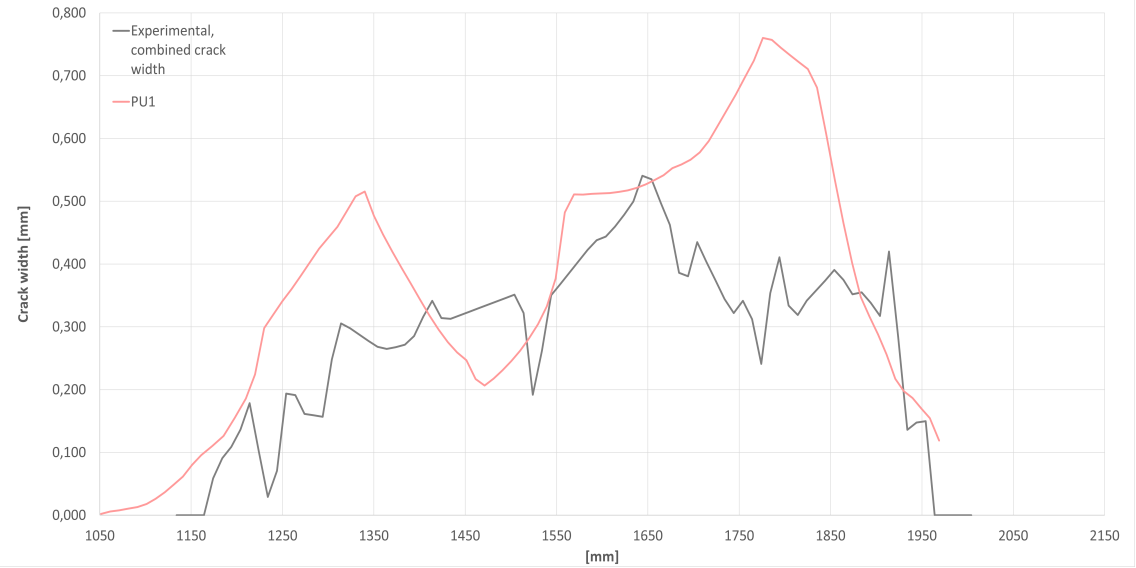

Figure 5.4: Comparison between the crack width of the lateral side of PU1_FEA and the measured crack width from the experiment.

5.3 U1_FEA

In this analysis, corrosion distribution was modeled as uniformly spread along the corroded region. Crack initiation is first observed between the first and second bending crack on the lateral side. The final crack pattern does not correlate well with the final crack pattern of the experiment as the largest corrosion induced cracks are formed on the tensile side of the beam. This crack goes all the way between the third and 6^{th} bending crack. Overall the crack pattern of this case does not agree with the experiment.

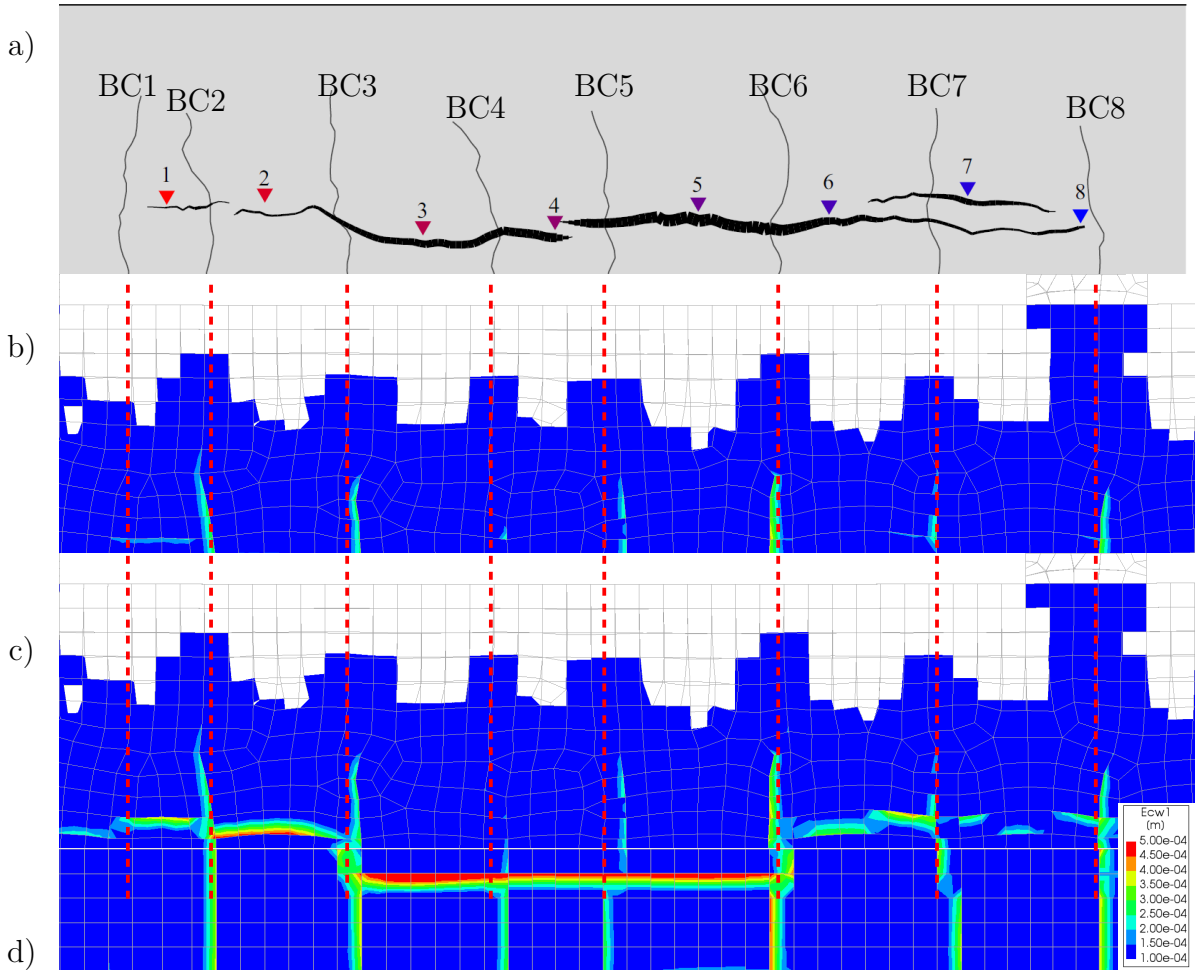

Figure 5.5: a) The recreated final crack pattern of the experiment. b) The crack pattern of the analysis after half the time has passed. c) and d) Represent the lateral and tensile side crack patterns at the end of the FE analysis. The numbers at the top of the image represent the numbering of the bending cracks. The triangles are where the experiment measured the crack widths with regards to time in the experiment, and dots where the crack widths of the tensile side was measured with regards to time.

Figure 5.6: Comparison between the crack width of the lateral side and the corrosion distribution of Bar 1 in U1_FEA

Examining the maximum crack widths depicted in Figure 5.6, it can be clearly seen that even though corrosion is constant along the corroded region the measured crack widths are not. In Figure 5.7 neither the shape or the final crack widths on the lateral side does not resemble the experimental measurements in this case. The significant drop in crack widths on the lateral side between 1350mm and 1700mm can be attributed to the corrosion induced crack forming on the tensile side instead of on the lateral side.

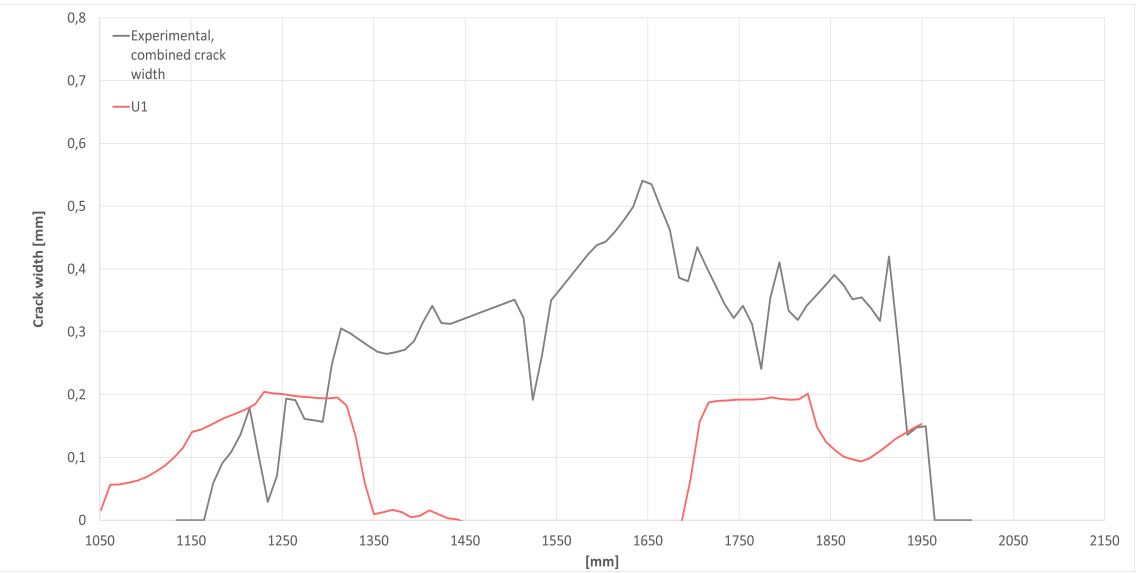

Figure 5.7: Comparison between the crack width of the lateral side of U1_FEA and the measured crack width from the experiment.

5.4 UO1_FEA

The crack pattern of UO1_FEA is presented in 5.8 and here the initiation of cracks is happening only in the regions between the bending cracks. The final crack pattern does not show substantial amounts of corrosion induced cracking as the cracking occurs between the 6^{th} and 7^{th} bending crack on the lateral side of the beam. Cracking also occurs on the tension side of the beam between the 7^{th} and 8^{th} bending crack. The sudden change in which side the corrosion induced crack forms could be due to the presence of the stirrup close to the 7^{th} bending crack, preventing the cracking of the lateral side.

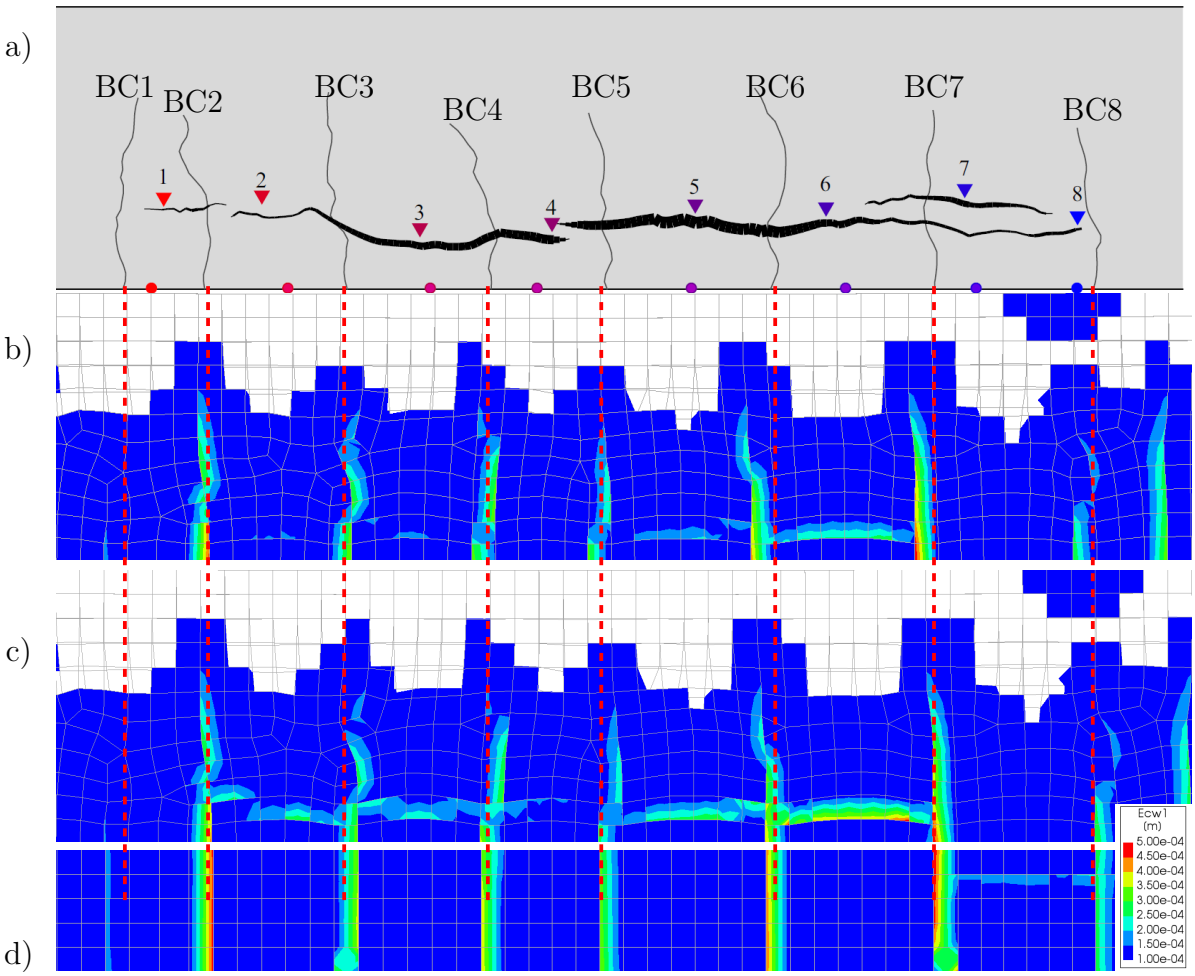

Figure 5.8: a) The recreated final crack pattern of the experiment. b) The crack pattern of the analysis after half the time has passed. c) and d) Represent the lateral and tensile side crack patterns at the end of the FE analysis. The numbers at the top of the image represent the numbering of the bending cracks. The triangles are where the experiment measured the crack widths with regards to time in the experiment, and dots where the crack widths of the tensile side was measured with regards to time.

Figure 5.9: Comparison between the crack width of the lateral side of UO1_FEA and the corrosion distribution (corrosion depth) of Bar 1 in UO1_FEA.

In Figure 5.9 there seems to be a clearer correlation between the level of corrosion and the measured crack widths on the lateral side of the beam. The highest crack widths correspond with the largest measured crack widths. Comparing the crack widths of the FE analysis and the experimental data, seen in Figure 5.10 the crack widths are significantly lower. The cracking of the lateral side is prevented much earlier than in the experiment (around 1850mm) which could indicate a different location of the stirrup than what was present in the experimental beam.

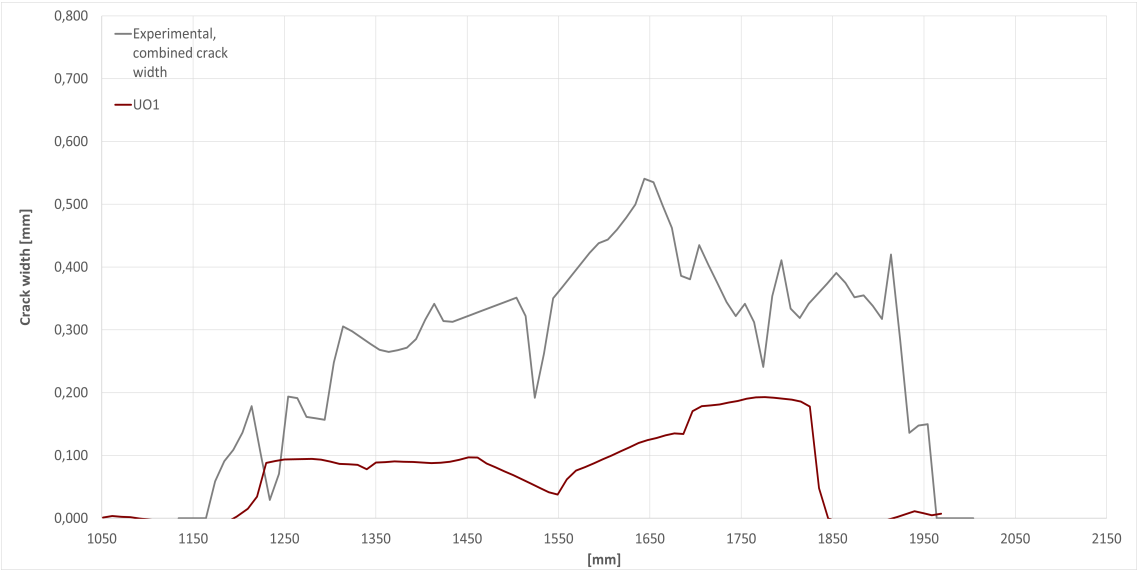

Figure 5.10: Comparison between the crack width of the lateral side and the measured crack widths of the experiment. In this figure the positions of the crack widths are adjusted to start at same location of those measured in the FE analysis

5.5 Effect of varying volume expansion

Since volume expansion can differ depending on the corrosion products produced by the corrosion, analysis of varying the volume expansion on the corrosion products was made. The volume expansion was changed for each corrosion distribution to see the effects the volume expansion has on each distribution. The first presented is the PU_FEA in which includes both pitting and uniform corrosion between the bending cracks which is presented in 5.11. Secondly the corrosion distribution applied as an average corrosion along the corroded region presented in 5.12, and thirdly where the pitting corrosion is removed and replace by non corroded sections presented in 5.13.

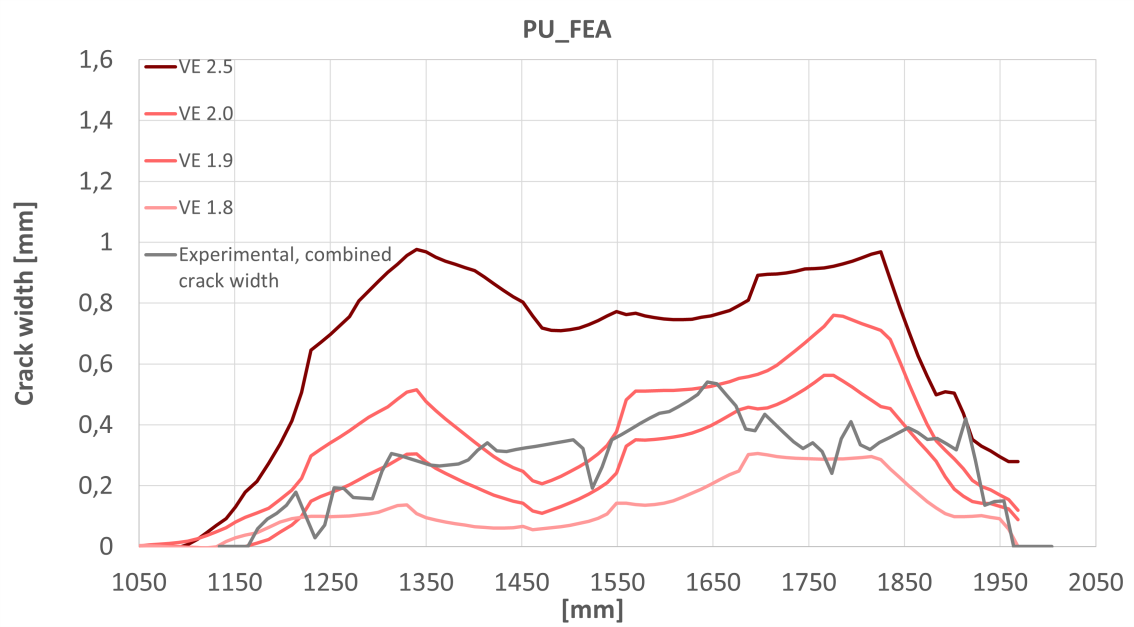

Figure 5.11: A comparison between the crack widths of each PU_FEA to see how the crack widths change when varying the volume expansion.

The effects the volume expansion have on the measured crack widths PU_FEA is very consistent. The overall shape of the graph stay the same when increasing the degree of volume expansion. However, as the volume expansion becomes large the sections with the highest crack width does not correspond with the highest amount of corrosion present. Local effects of pitting corrosion appears to be spreading out into the nearby sections.

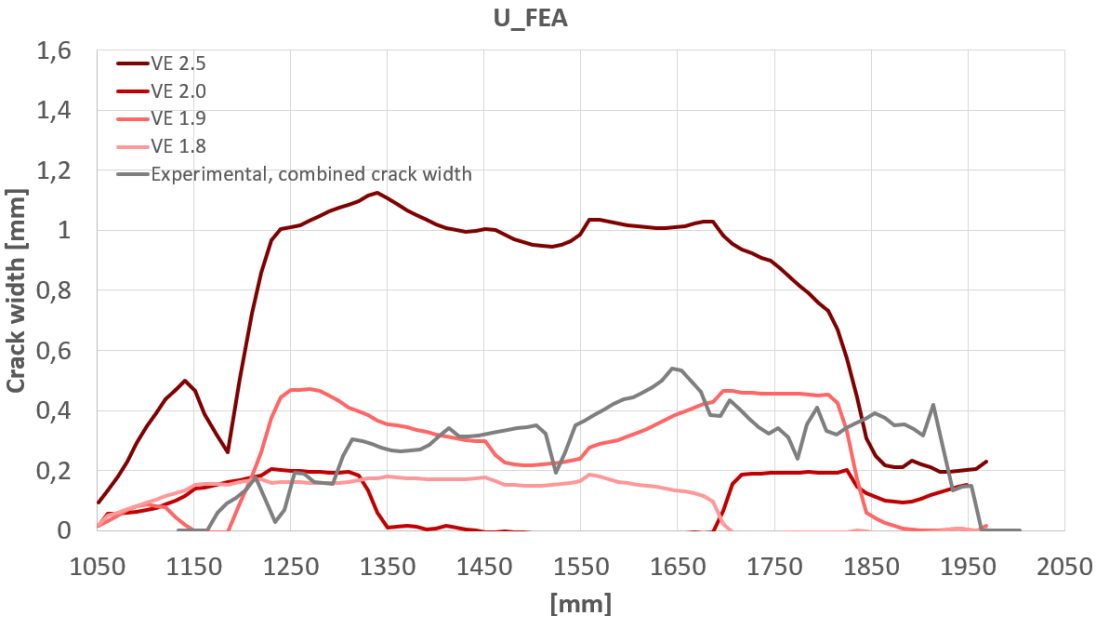

Figure 5.12: A comparison between the crack widths of each U_FEA to study how the crack widths change when varying the volume expansion.

In the analyses with corrosion was distributed as the average corrosion over the corroded region, the volume expansion change the pattern of the measured crack widths. Almost no correlation of the shape is present between any of the FE analyses. This indicates a very non-linear relation between the crack widths along the cracked region and the volume expansion of the corroded model when the corrosion are kept constant along the corroded region. This could be due to other effects taking over the determination of the crack formation and crack widths when there is no change in corrosion distribution.

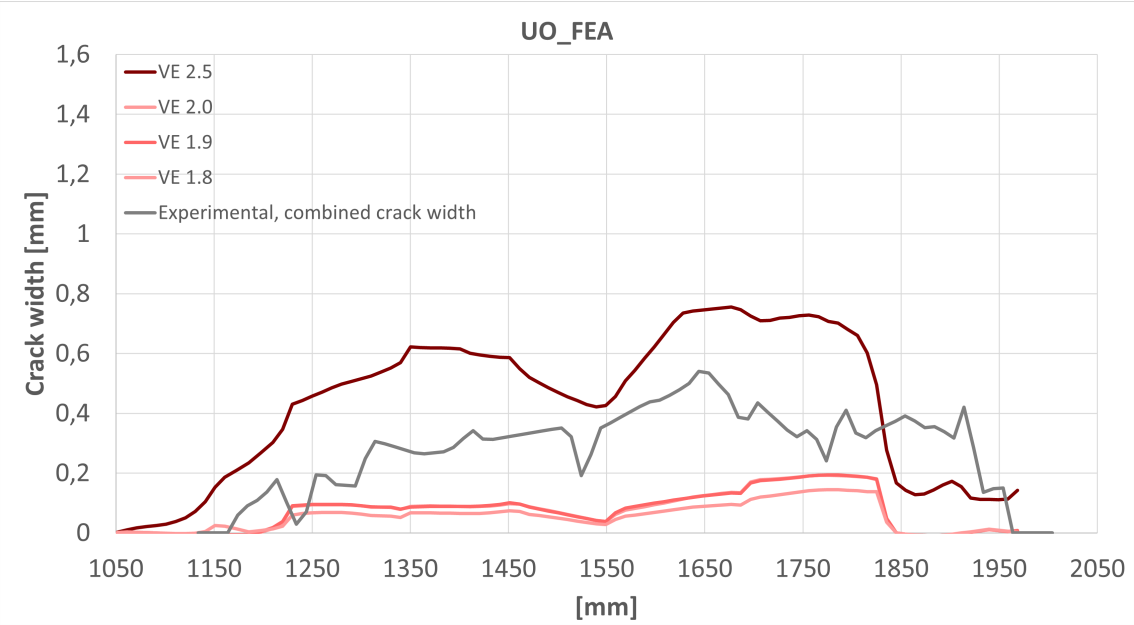

Figure 5.13: A comparison between the crack widths of each UO_FEA to study how the crack widths change when varying the volume expansion.

Two observations can be made from Figure 5.13 when varying the volume expansion in the analysis with pitting corrosion removed. First, there are minimal increases in crack widths when transitioning from 1.8 to 2.0 but overall pattern between the three are consistent. Increasing the crack width to 2.5 show a larger change in the shape of the graph. It also starts to more resemble the shape of the experiment although with somewhat higher measured crack widths. As the crack widths gradually grow from the left to right with a dip in the measured crack widths around 1550mm. As stated before the sudden drop in crack widths compared with the experimental results could be due to the different placement of the stirrup in the FE-model than in the experiment.

5.6 Crack widths and time

In the experiment the growth of the crack widths were shown to have a linear expansion during the corrosion process. Therefore it would be of high interest to know if the longitudinal crack widths grow in the same way in the FE analysis since we know that the corrosion are applied as one hundredth of the final corrosion depth for each time step. Therefore if the growth of crack widths are linear, then there is a direct correlation between an increase in corrosion and the longitudinal crack width. In figure 5.14 the location at which the corrosion-induced cracks were measured with respect to time in the experiment as well as FE analysis is presented together with the corrosion depth applied in the FE analysis. The numbering of the measured locations are the corresponding numbering in figure 5.15 and 5.16. In the experiment, the corrosion process was halted for some time. This period have been removed in the following figures and one can therefore observe a sudden increase or decrease of the measured crack widths of the experiment which occurs at 35 days

of figure 5.15 and 5.16. A limitation was made to limit the measured locations as in the experiment the amount of measured locations were 8 but is limited to the 5 presented in figure 5.14. This was done for the graph to be easier to read as the other measurements either had no present cracks or showed the same behaviour. U1_FEA was also not considered as the corrosion induced crack distribution was more present on the tension side and not on the lateral side as in the experiment.

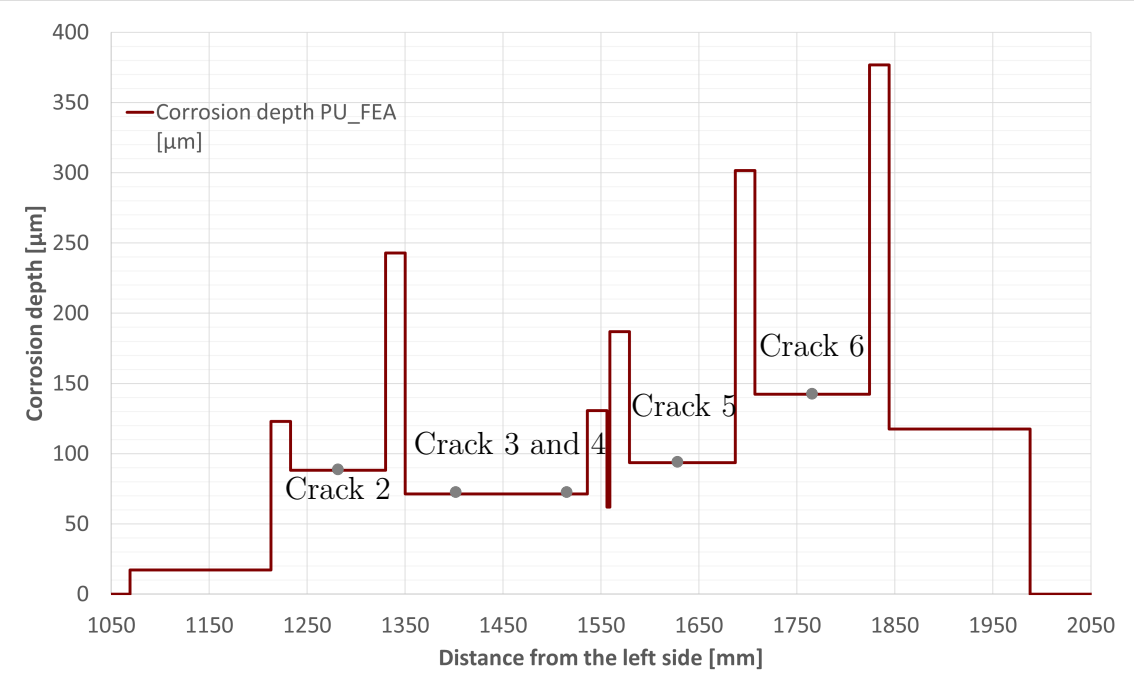

Figure 5.14: Corrosion depth of Bar 1 together with the measured location (on the lateral side of the beam) of crack widths with regards to time in the experiment and FE analysis represented by gray dots.

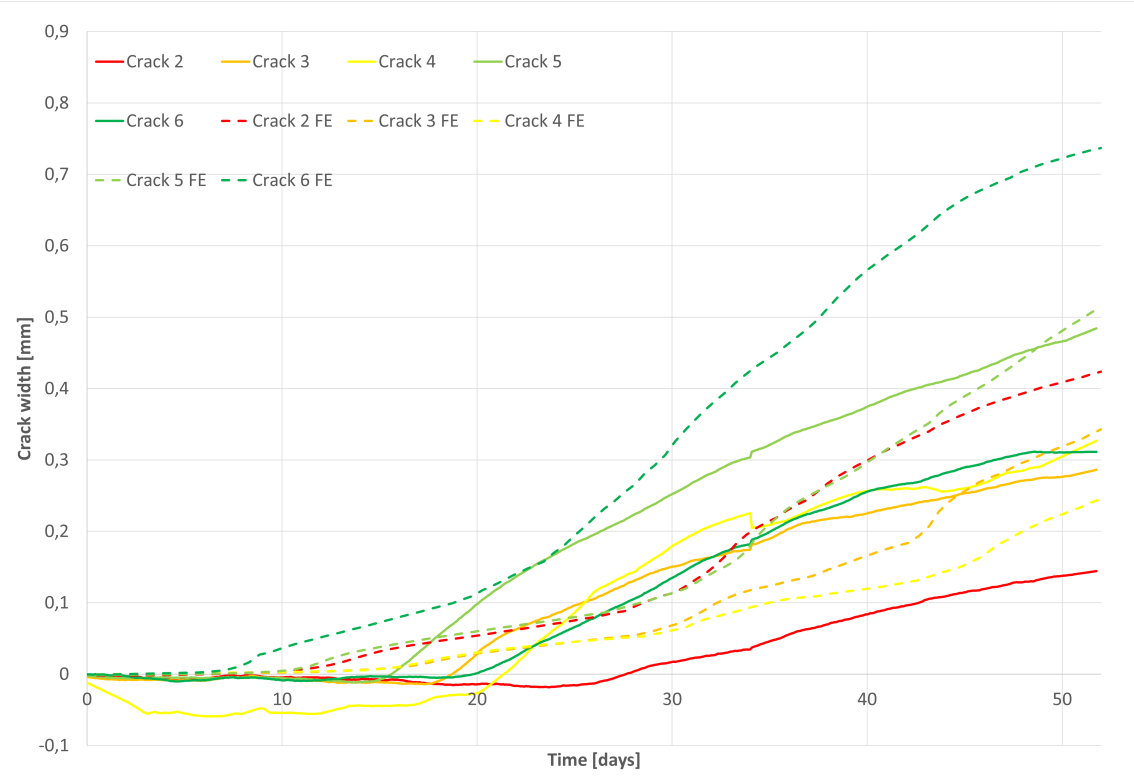

Figure 5.15: Crack width growth of the FE analysis PU1_FEA.

In the figure 5.15 the growth of the crack at the same location as was measured in the experiment of PU1_FEA is presented. The growth have more or less two phases based on the data of the FE analysis. The crack width grow in a linear manner up until around 0.1 to 0.2 mm in crack width. After this the propagation of the crack width starts growing with an increased rate and does not maintain the linear relation at every measured location as was can be observed in the first phase.

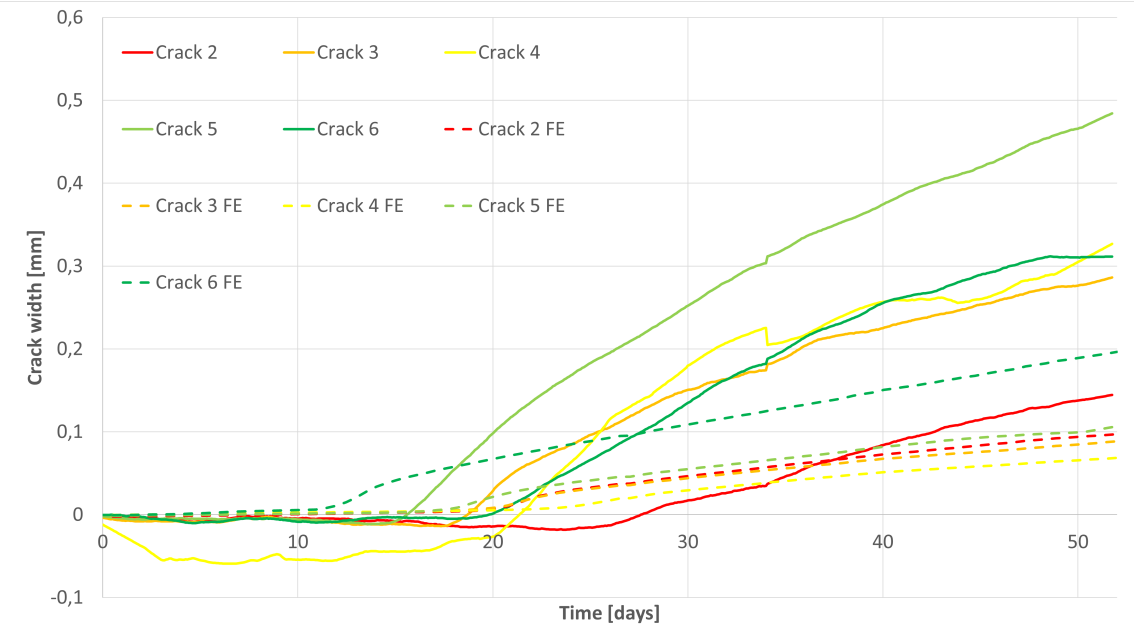

Figure 5.16: Crack width growth of the FE analysis UO1_FEA.

In the case where pitting corrosion was removed, the crack propagation is presented in Figure 5.16. Here the linear relation between crack width growth and time is present. So the linear relation between time and crack propagation as was observed in the experiment is reproduced in this analysis. However as stated before, the final crack widths are much lower than those measured in the experiment.

6
Discussion

The final crack pattern of the FE analysis where the corrosion was modelled as close to what was measured in the experiment shows the highest correlation in terms of crack pattern on the lateral side of the beam. In the other two, the crack pattern were otherwise much different in terms of lower crack widths or a larger crack forming on the tension side of the beam as in the case of U1_FEA. Crack initiation occurred between the bending cracks in all three corrosion distributions. However, cracking at the bending cracks was also observed initiating in PU1_FEA at the 6^{th} and 7^{th} bending crack. Minor cracking of the tensile side was also seen in UO1_FEA between the 7^{th} and 8^{th} and could most likely be explained by the presence of the stirrup located in this region. This is also the same location as some cracking of the tensile side can be observed in PU1_FEA. Overall the model appeared to be good at reproducing the overall final crack pattern of the experiment with corrosion distribution modelled as what was measured in the experiment. However, the model where the pitting corrosion was removed reproduced better the formation of cracks only occurring between the bending cracks. Suggesting the crack initiation in the experiment was mostly due to the uniform corrosion between the bending cracks, and not by the pitting corrosion.

None of the analyses with a volume expansion of 2.0 showed any clear correlation or matching with the results of the experimental data. Only the analysis where pitting corrosion was removed with volume expansion of 2.5 showed the highest correlation in terms of the graph pattern although with higher measured crack widths. This pattern is also observed with the lower volume expansions with the same corrosion distribution. This could indicate that the corrosion distribution that mimics the dissipation of corrosion products through the bending cracks better reproduce the cracking behaviour of the experiment. PU_FEA showed overall no resemblance with the shape of the crack width pattern. This is also observed in U_FEA where the crack widths also showed no resemblance with the crack width measurements of the experiment. This analysis did however show even though corrosion depth was constant along the entire corroded region, that the crack width pattern differs between each degree of volume expansion. If the beam was not under imposed deformation and not subjected to bending cracks, the crack widths should stay constant along the corroded region. Instead we see variations of crack widths, suggesting, that the corrosion of the reinforcement is not the only parameter affecting the corrosion-induced crack widths and crack pattern. The bending cracks, bending and subsequent curvature of the beam could have a part to play in the final crack widths and crack pattern.

In the analyses where the corrosion was modelled as close to the experiment (PU_FEA), pitting corrosion increased the crack widths at and around the pit location, with diminishing effects as one moved further away from the pit. Consequently, if pitting corrosion occurred at two bending cracks, the crack widths between the bending cracks appear to also increase which could lead to increased chance of cracking between the bending cracks. However, cracks were still observed between the bending cracks when pitting corrosion was removed, indicating that the crack widths in these regions are also dependent on the occurrence of the corrosion present between each pit. This observation may explain the previous scatter and the challenge of establishing a direct connection between pitting corrosion and longitudinal crack widths between bending cracks as well as the connection between local corrosion level and crack width. The effects corrosion has on longitudinal crack widths appear to radiate out from its origin and diminishing the further away from the location of corrosion. Therefore the corrosion induced crack widths are dependent on several factors that interplay and results in the measured crack widths. Furthermore, the analyses indicates as discussed by Berrocal et. al. [11] that a reason for crack initiation occurring only between the bending cracks in the experiment, could have been due to the dissipation of corrosion products in the pits through the bending cracks. Therefore not contributing to the corrosion-induced crack initiation. Further complicating the connection between corrosion levels and observed corrosion-induced crack propagation on the concrete cover. Further research on the effect of dissipation of corrosion products in experiments like those conducted by Berrocal et. al. [11] would help in the understanding of corrosion-induced crack initiation.

The effect stirrups have on the cracking of the lateral side of the beam can be seen on all the analyses of U_FEA and UO_FEA where there is a significant drop in crack width around 1850mm due to the presence of a stirrup. This stirrup prevents the cracking of the lateral side. The discrepancy between the lateral cracks at the ends could be due to the stirrups not being placed at the same location in the FE analysis as was in the experiment. As no information on the exact location of the stirrups was provided in Berrocal et. al. [11]. The crack pattern of UO_FEA shows some resemblance with the experimental data with a volume expansion of 2.5 although slightly higher and offset to the left. The crack widths of the FE analysis increases gradually from left to right and peaks around 1650. The FE analysis however also show a much larger drop in crack widths around 1550mm although still a drop around the same location.

Furthermore, it should be noted that the stress-strain relationship of the corrosion model differed between the original model proposed by Lundgren [26] (set at 7 MPa) and the analysis using the value of the updated model [27, 10] (using a value of 14 MPa), which might have affected the observed crack widths. A model which employs the original value could produce crack widths more in line with experimental data.

The variation of volume expansion appear to have a non-linear effect on the shape and the measured crack widths on the lateral side of the beam. As can be seen

in all three corrosion distributions, changing the degree of volume expansion can lead to more or less increases in crack widths between different measured areas. Two analyses that kept the shape and crack widths very consistent was UO1_FEA, UO4_FEA and UO5_FEA as is seen in figure 5.13. The pattern is best preserved between each degree of volume expansion in in PU_FEA. No analysis did however completely reproduce the crack widths measured in the experiment so it appears that the FE model can consistently recreate the crack pattern of the lateral side of the experiment well, given the corrosion distribution as it was measured in the experiment. However, the crack widths and crack propagation of the experiment differs much more compared with the experimental results. Showing that the model could be good at recreating the overall crack pattern and crack initiation, but not the specific crack widths at a given location. This could be due to the models inability to reproduce certain real world effects such as the dissipation of corrosion products through the opening of a crack and thereby decreasing the effects the corrosion products have on crack propagation.

In the experiment the crack widths had a linear relation between crack width and time. This was however not present in any of the analyses. The crack width growth rate are not constant throughout the analysis. At first the growth relation with time is linear, but this changes and the cracks starts growing faster in PU1_FEA. Towards the end of the analysis the growth of crack widths at some of the measured locations appeared to even be slowing down. The growth of crack widths in the analysis UO1_FEA showed more resemblance with the growth of crack widths in the experiment and especially the final crack widths. It can be observed in figure [5.16] that the crack widths evolve linearly throughout the whole analysis. So when cracks are small the FE analysis show that the crack width grows linearly, but as they become larger, the growth rate increases. This difference compared with the experiment could be explained by the fact that when a crack opens, the corrosion inside can dissipate through the crack. This effect can not be modelled in the FE analysis in any other way than reducing the corrosion depth. So even though corrosion rate might even be increased by the opening of the crack, the growth of the crack width does not increase as the corrosion products can dissipate through the longitudinal cracks. This could explain the absence of a linear relation between crack width growth and time throughout the whole analysis.

7
Conclusion

In this project, finite element analyses were conducted to investigate the cracking pattern of a reinforced concrete beam subjected to imposed deformation and corrosion. The FE analyses were compared among themselves and with available test results. Imposed deformation was applied to induce cracks, followed by the application of a corrosion model to simulate the volume expansion of steel during corrosion. The swelling action of uniform corrosion and pitting corrosion was modeled by interface elements between the steel and concrete, and the cross-sectional loss was varied along the corroded region to simulate the observed corrosion on the reinforcement in the test. Based on these analyses, the following conclusions have been drawn:

- The non-linear finite element analysis successfully reproduced the cracking pattern observed in the experiment.
- When pitting corrosion is included, corrosion-induced cracks are initiated both in between, and at the bending cracks.
- Corrosion-induced cracks initiate primarily between the bending cracks when pitting corrosion is removed or when corrosion is spread evenly along the corroded region.
- The FE analysis agrees with experimental results that the most corroded section does not necessarily cause the largest crack widths.
- The effect of volume expansion on the crack widths appears to be non-linear as the increase or decrease of the volume expansion does not lead to the same change in crack widths along the entire cracked region.
- Pitting corrosion causes an increase in longitudinal crack width at the location of the pit, with its influence decreasing further away from the pit.
- The initiation of cracks between bending cracks was primarily driven by uniform corrosion between the bending cracks.
- The FE analysis reproduced the linear crack growth with respect to time as observed in the experiment when cracks are small.

7.1 Suggestions for Future Research

To enhance the understanding of the corrosion-induced crack pattern and crack width in relation to imposed deformation and bending cracks, it is essential to incorporate more test data in future research. This could involve conducting tests with varying levels of imposed deformation to gather a broader range of results. By doing so, valuable insights can be gained regarding the influence of these factors on the

longitudinal crack development. Moreover, to gain a comprehensive understanding of the crack development and its relationship with corrosion, additional experiments could be performed to examine the corrosion rate at different points in time. This would also help determine the extent to which longitudinal cracks depend on pitting corrosion or uniform corrosion between pits. This study revealed that neither pitting corrosion nor uniform corrosion between the bending cracks alone could fully explain the observed crack widths and cracking pattern of the FE analysis. It would also be of interest to investigate in a future experiment and more FE analyses on the effects of dissipation of corrosion products through bending cracks. Furthermore, the impact of stirrups on the lateral cracking could be looked into as well since the stirrups could be one key contributor to the crack pattern on the edge of the corroded region not matching the experimental crack pattern and crack widths. Additionally, to further increase the knowledge of how corrosion-induced cracks are created by the corrosion model: FE analyses with less randomized locations of pitting corrosion and bending cracks should be made. In order to more clearly see how a pit or a bending crack influences the measured longitudinal crack widths on the concrete cover.

In summary, future work should focus on including more test data with varying levels of imposed deformation, conducting additional tests to examine the corrosion rate, dissipation of corrosion products and conducting further analysis to explore the effects of curvature and looking into the impacts of stirrups on lateral side cracking. Additionally, running less varied FE analyses on where the bending cracks and pit locations are more controlled to see how they affect the measured longitudinal crack widths. These efforts will lead to a deeper understanding of the factors influencing the corrosion induced crack pattern and crack widths in reinforced concrete beams.

Bibliography

[1] M. F. Montemor, A. M.P. Simões, and M. G.S. Ferreira. Chloride-induced corrosion on reinforcing steel: From the fundamentals to the monitoring techniques, 2003.

[2] H Peter Golter, John Kennedy, Tanya Wattenburg Komas, Jessi Meyer, Matthew Petree, Bryan Smith, Stephan Trepanier, David Whitmore, and Pat Winkler. Sustainability for repairing and maintaining concrete and masonry buildings, 2014.

[3] Mark G. Stewart, Xiaoming Wang, and Minh N. Nguyen. Climate change impact and risks of concrete infrastructure deterioration. *Engineering Structures*, 33:1326–1337, 4 2011.

[4] American Society of Civil Engineers. A comprehensive assessment of america's infrastructure, 2021.

[5] Maurizio Morgese, Farhad Ansari, Marco Domaneschi, and Gian Paolo Cimellaro. Post-collapse analysis of morandi's polcevera viaduct in genoa italy. *Journal of Civil Structural Health Monitoring*, 10:69–85, 2 2020.

[6] Luca Bertolini, Bernhard Elsener, Pietro Pedeferri, Elena Redaelli, and Rob B Polder. *Corrosion of Steel in Concrete : Prevention, Diagnosis, Repair*. 2nd edition, 2013.

[7] Y. Zhou, B. Gencturk, K. Willam, and A. Attar. Carbonation-induced and chloride-induced corrosion in reinforced concrete structures. *Journal of Materials in Civil Engineering*, 27, 9 2015.

[8] Wenjun Zhu and Raoul François. Structural performance of rc beams in relation with the corroded period in chloride environment. *Materials and Structures/-Materiaux et Constructions*, 48:1757–1769, 6 2015.

[9] Ignasi Fernandez, Jesús Miguel Bairán, and Antonio R. Marí. Corrosion effects on the mechanical properties of reinforcing steel bars. fatigue and - behavior. *Construction and Building Materials*, 101:772–783, 12 2015.

[10] K Lundgren. Bond between ribbed bars and concrete. part 2: The effect of corrosion, 2005.

[11] Carlos G. Berrocal, Ignasi Fernandez, and Rasmus Rempling. The interplay between corrosion and cracks in reinforced concrete beams with non-uniform reinforcement corrosion. *Materials and Structures/Materiaux et Constructions*, 55, 5 2022.

[12] Chuanqing Fu, Nanguo Jin, Hailong Ye, Xianyu Jin, and Wei Dai. Corrosion characteristics of a 4-year naturally corroded reinforced concrete beam with load-induced transverse cracks. *Corrosion Science*, 117:11–23, 3 2017.

[13] E. Chen, Carlos G. Berrocal, Ingemar Löfgren, and Karin Lundgren. Correlation between concrete cracks and corrosion characteristics of steel reinforcement in pre-cracked plain and fibre-reinforced concrete beams. *Materials and Structures/Materiaux et Constructions*, 53, 4 2020.

[14] E. Chen, Carlos G. Berrocal, Ingemar Löfgren, and Karin Lundgren. Comparison of the service life, life-cycle costs and assessment of hybrid and traditional reinforced concrete through a case study of bridge edge beams in sweden. *Structure and Infrastructure Engineering*, 19:39–57, 2022.

[15] Y. Z. Wang, Y. X. Zhao, F. Y. Gong, J. F. Dong, and Koichi Maekawa. Developing a three-dimensional finite element analysis approach to simulate corrosion-induced concrete cracking in reinforced concrete beams. *Engineering Structures*, 257, 4 2022.

[16] J. p. Broomfield. *Corrosion of steel in concrete: understanding, investigation and repair*. E FN Spon., 1 edition, 1997.

[17] Kyösti Tuutti. *Corrosion of steel in concrete*. Swedish Cement and Concrete Research Institute, 1982.

[18] Amin Jamali, Ueli Angst, Bryan Adey, and Bernhard Elsener. Modeling of corrosion-induced concrete cover cracking: A critical analysis, 2013.

[19] Linwen Yu, Raoul François, Vu Hiep Dang, Valérie L'Hostis, and Richard Gagné. Distribution of corrosion and pitting factor of steel in corroded rc beams. *Construction and Building Materials*, 95:384–392, 7 2015.

[20] Abdullah A. Almusallam, Ahmad S. Al-Gahtani, Abdur Rauf Aziz, and Rasheeduzzafar. Effect of reinforcement corrosion on bond strength. *Construction and Building Materials*, 10:123–129, 3 1996.

[21] Carlos G. Berrocal, Ingemar Löfgren, and Karin Lundgren. The effect of fibres on steel bar corrosion and flexural behaviour of corroded rc beams. *Engineering Structures*, 163:409–425, 5 2018.

[22] Carl Lindqvist and Franklin Milan Gotame. Fe analyses of strengthened concrete beams with corroded reinforcement, 2021.

[23] Milan Gotame, Carl Lindqvist Franklin, Mattias Blomfors, Jincheng Yang, and Karin Lundgren. Finite element analyses of frp-strengthened concrete beams with corroded reinforcement. *Engineering Structures*, 257, 4 2022.

[24] Omar Darwish and Akash Roshan. Fe analyses of corrosion-damaged rc beams strengthened with frp components.

[25] D Coronelli and P Gambarova. Structural assessment of corroded reinforced concrete beams: Modeling guidelines. *Journal of Structural Engineering*, pages 1214–1224, 2004.

[26] Karin Lundgren. Bond between corroded reinforcement and concrete, 2001.

[27] K Lundgren. Bond between ribbed bars and concrete. part 1: Modified model k. lundgren bond between ribbed bars and concrete. part 1: Modified model, 2005.

[28] Mario Plos, Morgan Johansson, Kamyab Zandi, and Jiangpeng Shu. Recommendations for assessment of reinforced concrete slabs enhanced structural analysis with the finite element method, 2021.

[29] R V Milford and W C Schnobrich. Computational strategies for nonlinear and fracture mechanics problems: The application of the rotating crack model to the analysis of reinforced concrete shells, 1985.
[30] S J Foster and R I Gilbert. Rotating crack finite element model for reinforced concrete structures, 1996.
[31] H A W Cornelissen, D A Hordijk, and H W Reinhardt Summary. Experimental determination of crack softening characteristics of normalweight and lightweight concrete. *Institutional Repository*, 1 1986.
[32] Dong Chen and Sankaran Mahadevan. Chloride-induced reinforcement corrosion and concrete cracking simulation. *Cement and Concrete Composites*, 30:227–238, 3 2008.
[33] M. Tahershamsi, I. Fernandez, K. Zandi, and K. Lundgren. Four levels to assess anchorage capacity of corroded reinforcement in concrete. *Engineering Structures*, 147:434–447, 9 2017.
[34] En 12390-3:2009 testing hardened concrete. part 3: compressive strength of test specimens, 2009.
[35] Federation internationale du beton. *Fib model code for concrete structures 2010*.
[36] Eurocode 2: Design of concrete structures-part 1-1: General rules and rules for buildings, 2004.
[37] Beatrice Belletti, Cecilia Damoni, and Max A.N. Hendriks. Development of guidelines for nonlinear finite element analyses of existing reinforced and prestressed beams. *European Journal of Environmental and Civil Engineering*, 15:1361–1384, 2011.